

EFFECTS OF FALL-BACK ACCRETION ON PROTO-MAGNETAR OUTFLOWS IN GAMMA-RAY BURSTS AND SUPERLUMINOUS SUPERNOVAE

BRIAN D. METZGER¹, PAZ BENIAMINI², DIMITRIOS GIANNIOS³*Draft version February 17, 2022*

ABSTRACT

Rapidly spinning, strongly magnetized proto-neutron stars (“millisecond proto-magnetars”) are candidate central engines of long-duration gamma-ray bursts (GRB), superluminous supernovae (SLSNe), and binary neutron star mergers. Magnetar birth may be accompanied by the fall-back of stellar debris, lasting for seconds or longer following the explosion. Accretion alters the magnetar evolution by (1) providing an additional source of rotational energy (or a potential sink, if the propeller mechanism operates); (2) enhancing the spin-down luminosity above the dipole rate by compressing the magnetosphere and expanding the polar cap region of open magnetic field lines; (3) supplying an additional accretion-powered neutrino luminosity that sustains the wind baryon-loading, even after the magnetar’s internal neutrino luminosity has subsided. The more complex evolution of the jet power and magnetization of an accreting magnetar more readily accounts for the high ^{56}Ni yields GRB SNe and irregular time evolution of some GRB light curves (e.g. bursts with precursors followed by a long quiescent interval before the main emission episode). Additional baryon-loading from accretion-powered neutrino irradiation of the polar cap lengthens the timeframe over which the jet magnetization is in the requisite range $\sigma \lesssim 10^3$ for efficient gamma-ray emission, thereby accommodating GRBs with ultra-long durations. Though accretion does not significantly raise the maximum energy budget from the limit of $\lesssim \text{few} \times 10^{52}$ ergs for an isolated magnetar, it greatly expands the range of magnetic field strengths and birth spin periods capable of powering GRB jets, reducing the differences between the magnetar properties normally invoked to explain GRBs versus SLSNe.

1. INTRODUCTION

Rapidly-spinning, strongly-magnetized neutron stars (NS) formed in core collapse supernovae (“millisecond proto-magnetars”) are promising candidates for the central engines of long-duration gamma-ray bursts (GRB; Usov 1992; Dai & Lu 1998; Wheeler et al. 2000; Zhang & Mészáros 2001; Thompson et al. 2004; Bucciantini et al. 2007; Uzdensky & MacFadyen 2007; Metzger et al. 2007, 2011; Mazzali et al. 2014; Vlasov et al. 2014, 2017; Beniamini et al. 2017) and hydrogen-poor superluminous supernovae (SLSNe; Kasen & Bildsten 2010; Woosley 2010; Dessart et al. 2012; Chatzopoulos et al. 2013; Metzger et al. 2014; Sukhbold & Thompson 2017). Powering a relativistic GRB jet by the magnetic dipole spin-down luminosity of an isolated (non-accreting) magnetar requires a large surface magnetic field strength of $B_d \gtrsim \text{few} \times 10^{15}$ G, while SLSNe instead typically require weaker fields of $B_d \lesssim \text{few} \times 10^{14}$ G (e.g. Metzger et al. 2015). This difference arises because the spin-down timescale over which the magnetar’s rotational energy $\gtrsim 10^{52}$ ergs is extracted must be short in GRBs to explain their typically observed durations of \lesssim tens of seconds. By contrast, substantially enhancing the optical luminosity of the supernova, as needed to explain SLSNe, instead requires the magnetar’s energy be deposited into a nebula behind the ejecta over longer timescales \gtrsim days, comparable to the photon diffusion timescale out of the ejecta.

A millisecond magnetar is also created from the coalescence of binary NSs (e.g. Price & Rosswog 2006; Siegel et al. 2013; Kiuchi et al. 2014). A merger remnant that avoids promptly collapsing into a black hole can power long-lived electromagnetic counterparts to the gravitational wave emission, either by supplying an additional source of mildly-relativistic radioactive kilonova ejecta (on timescales $\lesssim \text{few}$ s after the merger; Metzger et al. 2018), relativistic ejecta and prompt gamma-ray/X-ray emission (on timescales of $\sim 1 - 10^3$ s; e.g. Metzger et al. 2008b; Bucciantini et al. 2012; Rowlinson et al. 2013; Zhang 2013), or by enhancing the optical/X-ray emission of the kilonova via spin-down luminosity (on timescales \sim hours–days; Kulkarni 2005; Yu et al. 2013; Metzger & Piro 2014; Gao et al. 2015; Siegel & Ciolfi 2016a,b), analogous to a scaled-down version of SLSNe. The fact that no such emission was observed following the recent LIGO NS merger GW170817 (Abbott et al. 2017b,a) favored a relatively rapid black hole formation in this event (Margalit & Metzger 2017; Pooley et al. 2017; Margutti et al. 2018).

While the birth of millisecond magnetars can successfully reproduce many of the observed properties of GRBs (e.g. Metzger et al. 2011; Beniamini et al. 2017) and SLSNe (e.g. Nicholl et al. 2017; Yu et al. 2017), several outstanding challenges remain:

- **Energetics.** The total energy of the GRB and its afterglow in the magnetar model cannot exceed a fraction of the maximum rotational energy of a NS, which is $\sim 3 \times 10^{52}$ ergs for a canonical NS of mass $1.4M_\odot$ (Metzger et al. 2015; Beniamini et al. 2017). This limit is comparable to the measured or inferred energies of a handful of long GRBs and

¹ Department of Physics and Columbia Astrophysics Laboratory, Columbia University, New York, NY 10027, USA. email: bdm2129@columbia.edu

² Department of Physics, The George Washington University, Washington, DC 20052, USA

³ Department of Physics and Astronomy, Purdue University, 525 Northwestern Avenue, West Lafayette, IN 47907, USA

their afterglows (e.g. Cenko et al. 2011; Beniamini et al. 2015). It is also close to being violated by the very luminous optical transient ASASSN-15lh (Dong et al. 2016), which radiated $\gtrsim 10^{52}$ ergs and was identified as a SLSN (see, however Leloudas et al. 2016; Margutti et al. 2017).

- **Radioactive Nickel.** The broad-lined Type Ic supernovae which accompany long GRBs (e.g. Woosley & Bloom 2006; Liu et al. 2016) are inferred to produce a large quantity $\gtrsim 0.3M_{\odot}$ of ^{56}Ni (e.g. Mazzali et al. 2014). If this radioactive isotope is synthesized by shock-heating of the inner ejecta layers of the progenitor star to the requisite high temperatures $\gtrsim 5 \times 10^9$ K, then the kinetic luminosity of the central engine’s outflow must be $\gtrsim 10^{51} - 10^{52}$ ergs s^{-1} over the first $\lesssim 1$ s following the explosion (e.g. Suwa & Tominaga 2015; Wang et al. 2016; Barnes et al. 2017). Though an isolated magnetar with a very strong surface magnetic field $\gtrsim 10^{16}$ G can produce such a high jet luminosity, its rapid spin-down would leave the engine with little rotational energy remaining to power a luminous GRB jet over the following minute.⁴
- **Magnetar Parameters in GRB versus SLSNe.** The magnetic fields $B_d \gtrsim \text{few} \times 10^{15}$ G of magnetars required to explain the luminosities of long GRBs greatly exceed those $B_d \lesssim \text{few} \times 10^{14}$ G required to power SLSNe. As both models require similar birth spin periods, and the likely source of the strong magnetic field is the free energy available in rotation (e.g. Duncan & Thompson 1992), it is not clear what additional property gives rise to such a disparate range of magnetic field strengths (corresponding to a difference of a factor of $\gtrsim 100$ in magnetic energy of the dipole component). Many GRBs are also accompanied by extended X-ray plateaus (Burrows et al. 2006), which have been interpreted as being powered by the spin-down of long-lived magnetars (e.g. Zhang & Mészáros 2001); however, the magnetic field strength required to explain the plateau luminosity and duration are generally lower than those required to power the GRB jet at earlier times (Rowlinson et al. 2013; Gompertz et al. 2014; Rowlinson et al. 2014; Lü & Zhang 2014). Time-evolution of the magnetic field strength can be invoked, but fine-tuning may be required to account for the large energy of both the prompt and plateau phases (Beniamini & Mochkovitch 2017).
- **Ultra-Long GRBs.** In addition to canonical long GRBs, a handful of bursts with much longer durations $\gtrsim 10^3$ s have been discovered (Gendre et al. 2013; Levan et al. 2014; Boër et al. 2015; Levan 2015). It remains debated whether these “ultra-long GRBs” are simply the long-duration tail of a single long GRB population, or whether

they represent a distinct class with potentially different progenitors. One clue was provided by GRB 111209A, a ultra-long burst of duration $T_{\text{GRB}} \approx 10^4$ s, followed by a supernova with a luminosity between those of normal GRB SNe and SLSNe (Greiner et al. 2015; Kann et al. 2016). Metzger et al. (2015) showed that the same magnetar engine, with a magnetic field strength $B_d \approx 3 \times 10^{14}$ G and dipole spin-down timescale of $t_{\text{sd}} \sim 10^4$ s $\sim T_{\text{GRB}}$, could in principle power both a GRB jet (at the observed luminosity and duration) while also enhancing the luminosity of the subsequent supernova to the observed level (see also Gompertz & Fruchter 2017; Margalit et al. 2018).

However, the production of a jet with the correct power output and timescale is of itself not sufficient to explain the prompt gamma-ray emission; the jet magnetization σ , which is inversely proportional to the baryon loading (see eq. 28 for definition), must also lie in a critical range $100 \lesssim \sigma \lesssim 3000$ for the jet’s Poynting flux to be efficiently converted into MeV radiation (e.g. Beniamini & Giannios 2017). Following the supernova explosion, a proto-NS radiates its gravitational binding energy through neutrino emission during its Kelvin-Helmholtz contraction (Burrows & Lattimer 1986), becoming optically-thin to neutrinos on a timescale $t_{\text{thin}} \approx 10 - 30$ s (Pons et al. 1999). These neutrinos drive a substantial flux of baryons from the NS surface (Qian & Woosley 1996), keeping the jet magnetization in the optimal range to power GRB emission at times $\lesssim t_{\text{thin}}$; however, following the optically-thin transition $t \gtrsim t_{\text{thin}}$ the proto-NS neutrino luminosity plummets and the jet magnetization abruptly rises to enormous values (closer to those of normal pulsar winds), causing the prompt gamma-ray emission to cease (Metzger et al. 2011; Beniamini et al. 2017). While the agreement between t_{thin} and the durations of most long GRBs lends support to the magnetar model (Metzger et al. 2011), for the same reason it then becomes problematic to account for ultra-long GRBs with prompt emission lasting for times $T_{\text{GRB}} \gg t_{\text{thin}}$.

- **Irregular GRB Light Curves (e.g. Precursor Gaps).** Although all GRB light curves show variability, some of this behavior can be attributed to the central engine or variations in the jet properties imprinted by its propagation through the progenitor star (e.g. Morsony et al. 2010). However, some GRB light curves are characterized by initial “precursor” emission, which is followed by large gaps in time of up to hundreds of seconds before the onset of the main emission episode (e.g. Lazzati 2005; Wang & Mészáros 2007; Wu et al. 2013). Since the spin-down evolution of an isolated magnetar is relatively smooth, and is not expected to turn off for an extended period of time, such “gapped” light curve behavior is challenging to accommodate in the magnetar picture.

⁴ Though we note that the spin-down luminosity of even an isolated magnetar will not be constant at early times $\ll t_{\text{sd}}$, where t_{sd} is the spin-down time, if the open magnetic flux threading the magnetar surface shrinks as the wind magnetization grows in time (Bucciantini et al. 2006; see eq. 12).

This paper explores to what extent the above issues

can be alleviated by considering the effects of fall-back accretion on the evolution of millisecond magnetars and the properties of their relativistic jets. Core collapse supernovae are generally expected to leave a fraction of the stellar progenitor bound to the central compact object following the supernova explosion, which will fall-back over an extended period of time and circularize into an accretion disk (Chevalier 1989; Zhang et al. 2008; Fryer et al. 2009; Woosley & Heger 2012; Quataert & Kasen 2012; Perna et al. 2014). Binary NS mergers will also in general be accompanied by accretion from a remnant torus of high-angular momentum material (e.g. Fernández & Metzger 2013) and by delayed fall-back from the cloud of matter ejected by shocks and tidal forces dynamically during the merger (e.g. Rosswog 2007; Fernández et al. 2017).

One role of accretion is to supply additional angular momentum to the magnetar, in principle enhancing the reservoir of rotational energy available to power the GRB jet or SLSNe (Piro & Ott 2011; Bernardini et al. 2013, 2014; Gompertz et al. 2014). On the other hand, torques from the disk on the star may also result in the loss of stellar angular momentum if accretion occurs in the “propeller” regime. Likewise, the addition of too much mass will cause the magnetar to collapse to a black hole, abruptly truncating the source of the magnetar wind feeding the GRB jet (Rowlinson et al. 2010) or SLSNe (Moriya et al. 2016). By pushing the inner edge of the disk inside the light cylinder, a sufficiently high accretion rate acts to enhance the spin-down rate of the magnetar by opening up a large fraction of its magnetosphere (e.g. Parfrey et al. 2016) as well as increasing the baryon-loading of the jet through enhanced neutrino-heated outflows. These effects can change the temporal evolution of the magnetization and power of the GRB jet; the latter for instance no longer necessarily obeys the standard $\propto t^{-2}$ spin-down decay predicted at late times for an isolated magnetar.

This paper is organized as follows. In §2, we describe our model for the evolution of proto-magnetars and their relativistic jets, accounting for the effects of mass fall-back. In §3, we present our results for the magnetar spin-down evolution (§3.1) and implications for some of the issues raised above, including ^{56}Ni production in GRB SNe (§3.2), prompt gamma-ray emission (§3.3), GRBs with complex light curves such as long temporal “gaps” (§3.4), binary NS mergers (§3.5), and SLSNe (§3.6). In §4, we briefly summarize our conclusions.

2. MAGNETAR MODEL WITH ACCRETION

2.1. Fall-Back Accretion

The quantity and return rate of mass to the central neutron star following the core collapse of a massive star depends sensitively on the energy, asymmetry, and detailed mechanism of the explosion. Although large quantities of fall-back are rare in one-dimensional supernova models which undergo successful explosions (e.g. Ugliano et al. 2012; Sukhbold et al. 2016), fall-back in the equatorial plane defined by the angular momentum of the star may be more likely for polar-asymmetric MHD-powered explosions likely responsible for the birth of millisecond magnetars (e.g. Mösta et al. 2014). Mass accretion following the merger of two NSs also depends sensitively

on the properties of the initial binary, such as the mass ratio of its components (e.g. Hotokezaka et al. 2013). For simplicity, we assume a generic time-dependence for the mass fall-back rate of the form

$$\dot{M}(t) = \frac{2}{3} \frac{M_{\text{fb}}}{t_{\text{fb}}} \frac{1}{(1 + t/t_{\text{fb}})^{5/3}}, \quad (1)$$

where M_{fb} is the total quantity of returning mass and $t_{\text{fb}} \sim (G\bar{\rho})^{-1/2}$ is the characteristic fall-back time which depends on the mean density $\bar{\rho}$ of the layer of progenitor star contributing to M_{fb} . For example, the region just outside of the iron core ($\bar{\rho} \lesssim 10^8 \text{ g cm}^{-3}$) will fall back first, on a timescale $t_{\text{fb}} \sim$ seconds. The envelope of a compact stripped-envelope star ($\bar{\rho} \sim 1 - 100 \text{ g cm}^{-3}$) will return on a time $t_{\text{fb}} \sim 100 - 1000 \text{ s}$. More extended stars like blue supergiants ($\bar{\rho} \sim 10^{-5} - 10^{-3} \text{ g cm}^{-3}$) will have $t_{\text{fb}} \sim 10^5 - 10^6 \text{ s}$, while red supergiants ($\bar{\rho} \sim 10^{-7} \text{ g cm}^{-3}$) will have $t_{\text{fb}} \sim 10^7 \text{ s}$. A NS of initial mass $M_{\text{ns}} \approx 1.4M_{\odot}$ can accrete at most $M_{\text{max}} - M_{\text{ns}} \approx 0.6 - 0.8M_{\odot}$ before collapsing into a black hole (depending on the uncertain maximum mass of a NS, $M_{\text{max}} \gtrsim 2M_{\odot}$). Thus, depending on the progenitor star, we should consider accretion rates in the range $\dot{M} \sim M_{\text{fb}}/t_{\text{fb}} \sim 10^{-8} - 0.1M_{\odot} \text{ s}^{-1}$ acting over characteristic timescales ranging from seconds to months. Although the mass fall-back rate decays as $\propto t^{-5/3}$ at late times, the accretion rate reaching small radii may decay shallower in time $\dot{M} \propto t^{-4/3}$ if instead the dominant source of mass feeding is a viscously-spreading accretion disk (Metzger et al. 2008a).

Fall-back material with specific angular momentum $j_{\text{fb}} = (GM_{\text{ns}}R_{\text{fb}})^{1/2}$ will circularize into an centrifugally-supported torus outside the NS at the radius $\sim R_{\text{fb}}$ (we neglect possible complications arising from thermal pressure support behind the accretion shock; Milosavljević et al. 2012). For typical radial angular momentum profiles of the progenitor star, the shell-averaged value of $j_{\text{fb}}(r)$ increases with radius (Heger et al. 2005) and thus, as different layers of the star fall in, R_{fb} should increase monotonically with time (e.g. Kumar et al. 2008). For simplicity in what follows we assume that R_{fb} is roughly constant in time, motivated by the fact that most of the mass-fall back (arriving on the characteristic timescale $\sim t_{\text{fb}}$) originates from a given stellar layer with a roughly constant value of j_{fb} . We also assume that R_{fb} exceeds other critical radii in the problem, such as the light cylinder, co-rotation, and Alfvén radii, all of which are typically $\lesssim 100 \text{ km}$ for magnetar properties and accretion rates of interest (Table 1; §2.2). These assumptions can be generalized in future work, for instance to simultaneously account for the evolution of a viscously-spreading disk.

2.2. Critical Radii and Accretion Rates

The accretion disk extends inwards from its circularization point R_{fb} , feeding matter towards the NS at the rate \dot{M} . We neglect mass loss due to winds from the disk, as this can be accounted for by rescaling the effective value of the accreted mass M_{fb} in equation (1). The disk is truncated near the Alfvén radius R_{m} , as interior to this point the NS magnetosphere has a dominant influence over the accretion flow, directing the inflowing gas along field lines close to the edge of the polar funnel.

TABLE 1
CRITICAL RADII

Radius	Symbol	Value (km)
Neutron Star	R_{ns}	12
Light Cylinder	R_{lc}	$47.7 P_{\text{ms}}$
Co-Rotation	R_c	$16.8 P_{\text{ms}}^{2/3} M_{1.4}^{1/3}$
Alfvén	R_m	$22.2 B_{15}^{4/7} \dot{M}_{-2}^{-2/7} M_{1.4}^{-1/7}$

The magnetar is assumed to possess an equatorial surface dipole field strength of $B_d = B_{15} \times 10^{15}$ G and magnetic moment $\mu = B_d R_{\text{ns}}^3$ which is aligned with the rotation axis, where $R_{\text{ns}} = 12$ km is the NS radius. For an accretion rate $\dot{M} = \dot{M}_{-2} \times 10^{-2} M_{\odot} \text{s}^{-1}$, the Alfvén radius can be estimated as (e.g. Ghosh & Lamb 1978)

$$R_m = \left(\frac{3B_d^2 R_{\text{ns}}^6}{2\dot{M}\sqrt{GM_{\text{ns}}}} \right)^{2/7} \approx 22.2 B_{15}^{4/7} \dot{M}_{-2}^{-2/7} M_{1.4}^{-1/7} \text{ km}, \quad (2)$$

where $M_{\text{ns}} = 1.4 M_{1.4} M_{\odot}$ is the NS mass.

The central magnetar rotates with an angular frequency $\Omega = 2\pi/P$ and spin period $P = P_{\text{ms}} \times 1$ ms. Two additional key radii are the light cylinder radius,

$$R_{\text{lc}} = c/\Omega = 47.7 P_{\text{ms}} \text{ km} \quad (3)$$

and the co-rotation radius

$$R_c = \left(\frac{GM_{\text{ns}}}{\Omega^2} \right)^{1/3} \simeq 16.8 M_{1.4}^{1/3} P_{\text{ms}}^{2/3} \text{ km}. \quad (4)$$

These correspond, respectively, to the locations at which the azimuthal velocity of matter co-rotating with the magnetar equals the speed of light and the Keplerian velocity. These critical radii are summarized in Table 1.

As we describe below, the rate of magnetar spin-down due to angular momentum loss from a magnetized wind is enhanced when the Alfvén radius resides interior to the light cylinder. This condition ($R_m < R_{\text{lc}}$) is satisfied above a critical accretion rate of

$$\dot{M}_{\text{lc}} \simeq 6.9 \times 10^{-4} B_{15}^2 P_{\text{ms}}^{-7/2} M_{1.4}^{-1/2} M_{\odot} \text{s}^{-1}, R_m = R_{\text{lc}}, \quad (5)$$

or, correspondingly, below a spin period of

$$P_{\text{lc}} \simeq 0.47 B_{15}^{4/7} \dot{M}_{-2}^{-2/7} M_{1.4}^{-1/7} \text{ ms}. \quad (6)$$

The enhancement of the spin-down rate saturates once R_m is pushed all the way down to the NS surface, a condition that requires an even higher accretion rate of

$$\dot{M}_{\text{ns}} \simeq 0.086 B_{15}^2 M_{1.4}^{-1/2} M_{\odot} \text{s}^{-1}, R_m = R_{\text{ns}}, \quad (7)$$

Whether matter accretes freely onto the magnetar, or whether the system may enter the more complicated “propeller regime” (e.g. Romanova et al. 2003), depends on the location of the co-rotation radius relative to the Alfvén radius. R_m exceeds R_c for accretion rates above a critical value of

$$\dot{M}_c \simeq 0.026 B_{15}^2 P_{\text{ms}}^{-7/3} M_{1.4}^{-5/3} M_{\odot} \text{s}^{-1}, R_m = R_c \quad (8)$$

or, correspondingly, below a spin period of

$$P_c \simeq 1.52 B_{15}^{6/7} \dot{M}_{-2}^{-3/7} M_{1.4}^{-5/7} \text{ ms}. \quad (9)$$

These critical values of the accretion rate are summarized in Fig. 1 as a function of spin period for $B_d = 10^{15}$ G. The hierarchy $\dot{M}_{\text{lc}} \lesssim \dot{M}_c \lesssim \dot{M}_{\text{ns}}$ is preserved for all values of B_d and thus is generic also to the lower values of \dot{M} and B_d more relevant to SLSNe.

2.3. Magnetar Spin Evolution

The rotational energy of the magnetar is given by

$$E_{\text{rot}} = \frac{1}{2} I \Omega^2 \simeq 2.6 \times 10^{52} M_{1.4}^{3/2} P_{\text{ms}}^{-2} \text{ ergs}, \quad (10)$$

where I is the NS moment of inertia, which we approximate as $I \simeq 1.3 \times 10^{45} M_{1.4}^{3/2} \text{ g cm}^2$ (Fig. 1 of Lattimer & Schutz 2005). Maximum rotation energies of $E_{\text{rot}} \approx 3 \times 10^{52}$ ergs are typical for NSs of mass $1.4 M_{\odot}$ rotating near the break-up period of $P \simeq 1$ ms, but reservoirs up to $E_{\text{rot}} \approx 10^{53}$ ergs are possible for more massive NSs with $M_{\text{ns}} \gtrsim 2 M_{\odot}$ (Metzger et al. 2015).

Following the formation of a magnetar, its angular momentum $J = I\Omega$ evolves in time according to

$$\frac{dJ}{dt} = \dot{J}_{\text{acc}} - \dot{J}_{\text{sd}}, \quad (11)$$

where $\dot{J}_{\text{sd}} = \dot{E}_{\text{sd}}/\Omega$ accounts for losses due to the Poynting flux of the magnetized wind along the polar directions, and \dot{J}_{acc} accounts for gains or losses due to the torque from the accretion disk (see Fig. 2). We now discuss each of these processes in detail.

The magnetar loses rotational energy to a polar Poynting flux-dominated wind at a rate

$$\dot{E}_{\text{sd}} = \left(\frac{f_{\Phi}}{f_{\Phi, \text{lc}}} \right)^2 \frac{\mu^2 \Omega^4}{c^3}, \quad (12)$$

where we have assumed that the magnetic dipole and rotational axes are aligned (see Margalit et al. 2018 for generalization to the misaligned case). Here $f_{\Phi} = \int_0^{\theta_{\text{lc}}} \sin \theta d\theta \approx \theta_{\text{lc}}^2/2$ is the fraction of the magnetar surface threaded by open magnetic flux and θ_{lc} is the latitude from the pole of the last closed field line (e.g. Bucciantini et al. 2006). For an isolated pulsar wind, the closed field lines are typically assumed to extend to the light cylinder R_{lc} , corresponding to $\theta_{\text{lc}} \approx \sin^{-1}(R_{\text{ns}}/R_{\text{lc}})^{1/2} \approx (R_{\text{ns}}/R_{\text{lc}})^{1/2}$ (e.g. Contopoulos et al. 1999; Spitkovsky 2006), thus providing a minimum open flux of $f_{\Phi, \text{lc}} = R_{\text{ns}}/2R_{\text{lc}} \approx 0.13 P_{\text{ms}}^{-1}$. In this limit ($f_{\Phi} = f_{\Phi, \text{lc}}$), one recovers from equation (12) the normal magnetic dipole spin-down rate $\dot{E}_{\text{sd}} \propto \Omega^4$ of the force-free wind.

By contrast, for an accreting NS with $R_m \lesssim R_{\text{lc}}$, closed field lines are truncated where the disk begins, in which case $\theta_{\text{lc}} \approx (R_{\text{ns}}/R_m)^{1/2}$ and \dot{E}_{sd} is thus enhanced over

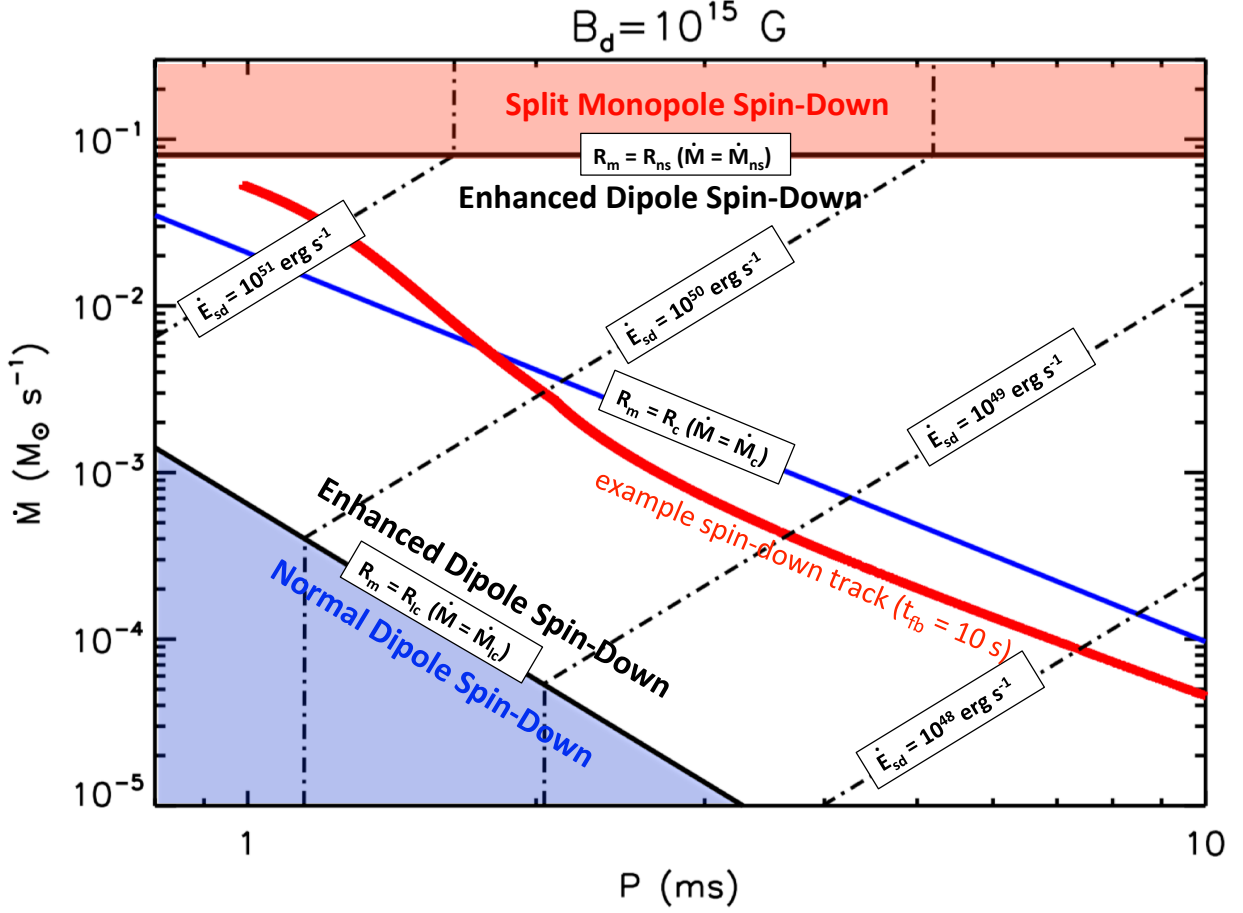


FIG. 1.— Regimes of magnetar spin-down evolution in the parameter space of mass accretion rate \dot{M} and spin period P , calculated for a magnetar of radius $R_{ns} = 12$ km, mass $M_{ns} = 1.4M_{\odot}$, and surface dipole magnetic field strength $B_d = 10^{15}$ G. Solid lines show accretion rates $\dot{M} = \dot{M}_{ns}$ (eq. 7), \dot{M}_c (blue; eq. 8), \dot{M}_{lc} (black; eq. 5). The condition $\dot{M} = \dot{M}_c$ approximately corresponds to the equilibrium spin period achieved if accretion spin-up is balanced by torques from the star-magnetosphere interaction (eq. 20). Dot-dashed lines show contours of constant spin-down luminosity \dot{E}_{sd} (eq. 13). A red solid line shows an example evolutionary track for an accreting magnetar ($t_{fb} = 10$ s shown in Fig. 3). Though we show results for a particular value of $B_d = 10^{15}$ G, all of the critical accretion rates scale as $\dot{M} \propto B_d^2$.

the standard dipole rate by a factor of $(R_m/R_{lc})^{-2} > 1$ (Parfrey et al. 2016). The maximum spin-down rate is achieved for the maximum open flux $R_m = R_{ns}$, i.e. the limit of a “split monopole” field geometry. Combining results, the wind energy loss rate is given by

$$\dot{E}_{sd} = \begin{cases} \frac{\mu^2 \Omega^4}{c^3} \frac{R_{lc}^2}{R_{ns}^2}, & \dot{M} \gtrsim \dot{M}_{ns}, \\ \frac{\mu^2 \Omega^4}{c^3} \frac{R_{lc}^2}{R_m^2}, & \dot{M}_{lc} \lesssim \dot{M} \lesssim \dot{M}_{ns}, \\ \frac{\mu^2 \Omega^4}{c^3}, & \dot{M} \lesssim \dot{M}_{lc} \end{cases},$$

$$\approx \begin{cases} 2.7 \times 10^{51} B_{15}^2 P_{ms}^{-2} \text{ ergs s}^{-1}, & \dot{M} \gtrsim \dot{M}_{ns}, \\ 8 \times 10^{50} B_{15}^{6/7} P_{ms}^{-2} \dot{M}_{-2}^{4/7} M_{1.4}^{2/7} \text{ ergs s}^{-1}, & \dot{M}_{lc} \lesssim \dot{M} \lesssim \dot{M}_{ns}, \\ 1.7 \times 10^{50} B_{15}^2 P_{ms}^{-4} \text{ ergs s}^{-1}, & \dot{M} \lesssim \dot{M}_{lc} \end{cases}, \quad (13)$$

Contours of fixed spin-down power are shown as dashed lines in Fig. 1.

A characteristic wind spin-down time is defined accord-

ing to

$$t_{sd} \equiv \frac{E_{rot}}{\dot{E}_{sd}} = \begin{cases} t_{sd,1} \simeq 9 B_{15}^{-2} M_{1.4}^{3/2} \text{ s}, & \dot{M} \gtrsim \dot{M}_{ns}, \\ t_{sd,2} \simeq 33 B_{15}^{-6/7} \dot{M}_{-2}^{-4/7} M_{1.4}^{17/14} \text{ s}, & \dot{M}_{lc} \lesssim \dot{M} \lesssim \dot{M}_{ns}, \\ t_{sd,3} \simeq 150 B_{15}^{-2} P_{ms}^2 M_{1.4}^{3/2} \text{ s}, & \dot{M} \lesssim \dot{M}_{lc} \end{cases} \quad (14)$$

When the accretion of mass or angular momentum from the disk can be neglected ($\dot{J}_{acc} = 0$, $dM/dt = 0$), and the accretion rate is constant in time, the magnetar spin-down $dE_{rot}/dt = -\dot{E}_{sd}$ exhibits a simple analytic solution in each of these regimes,

$$\dot{E}_{sd} = \begin{cases} \frac{E_{rot,0}}{t_{sd,1}} e^{-t/t_{sd,1}} & \dot{M} \gtrsim \dot{M}_{ns}, \\ \frac{E_{rot,0}}{t_{sd,2}} e^{-t/t_{sd,2}} & \dot{M}_{lc} \lesssim \dot{M} \lesssim \dot{M}_{ns}, \\ \frac{E_{rot,0}}{t_{sd,3}} (1 + t/t_{sd,3})^{-2} & \dot{M} \lesssim \dot{M}_{lc}, \end{cases} \quad (15)$$

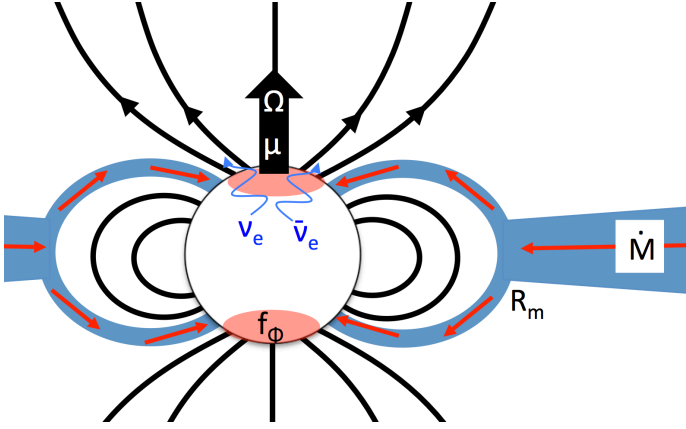


FIG. 2.— Schematic diagram of an accreting proto-magnetar and its magnetized relativistic outflow. The polar cap of open magnetic flux (shown in red) controls the spin-down rate of the magnetar and pollutes the jet with baryons. The rate of baryonic mass loss from the NS surface is controlled by neutrino heating in the proto-magnetar atmosphere ($\nu_e + n \rightarrow p + e^-$; $\bar{\nu}_e + p \rightarrow n + e^+$). The neutrinos arise both from the NS interior (until the NS becomes optically thin at times $t \lesssim t_{\text{thin}}$) and are produced in the magnetic accretion column, as shown in blue.

where $E_{\text{rot},0}$ is the initial rotational energy. Because both $t_{\text{sd},1}$ and $t_{\text{sd},2}$ are independent of the spin period, in these regimes the spin-down power decays as an exponential instead of the usual late-time power-law decay $\propto t^{-2}$ for dipole spin-down.

In addition to the losses from the magnetized wind, the magnetar can exchange angular momentum with the accretion disk at the rate (e.g. Piro & Ott 2011)

$$\dot{J}_{\text{acc}} = \begin{cases} \dot{M}(GM_{\text{ns}}R_{\text{ns}})^{1/2}(1 - \Omega/\Omega_K), & \dot{M} \gtrsim \dot{M}_{\text{ns}} \\ \dot{M}(GM_{\text{ns}}R_m)^{1/2}n(\omega) & \dot{M} \lesssim \dot{M}_{\text{ns}} \end{cases}. \quad (16)$$

Here the $(1 - \Omega/\Omega_K)$ factor in eq. 16 prevents the NS from gaining additional angular momentum once it is rotating near the centrifugal break-up velocity⁵ at $\Omega \approx \Omega_K = (GM_{\text{ns}}/R_{\text{ns}}^3)^{1/2}$.

Whether the disk spins up ($\dot{J}_{\text{acc}} > 0$) or spins down ($\dot{J}_{\text{acc}} < 0$) the magnetar will in general depend on the fastness parameter $\omega \equiv (R_m/R_c)^{3/2}$. The precise way that the torque changes around $\omega \approx 1$ is poorly understood and remains a matter of debate in the literature (e.g. D’Angelo & Spruit 2012). We explore two models for $n(\omega)$. First, as our fiducial case, we consider the prescription

$$n(\omega) = 1 - \omega, \quad \text{Piro \& Ott} \quad (17)$$

of Piro & Ott (2011), which allows for the loss of angular momentum from the NS in the so-called “propeller regime” $\omega \gtrsim 1$. On the other hand, Parfrey et al. (2016) argue for a minimal coupling between the NS magnetic field and the disk matter in the nominal propeller regime and instead take

$$n(\omega) = \begin{cases} 1, & \omega < 1 \\ 0 & \omega \geq 1. \end{cases} \quad \text{Parfrey} \quad (18)$$

As we show below, these different prescriptions can lead

⁵ Physically, this limit could be enforced by centrifugally-driven mass-loss or efficient gravitational wave losses induced non-axisymmetric instabilities which set in at high $T/|W|$ approaching the break-up threshold (e.g. Lai & Shapiro 1995).

to qualitative differences in the magnetar evolution, such as whether an equilibrium spin period is always achieved.

Accretion also causes the magnetar to grow in mass. How efficiently the star actually accepts the matter being fed from the disk depends on uncertain factors, such as whether the polar accretion column is able to cool through neutrinos and settle on the NS surface (Piro & Ott 2011). Another uncertainty is the efficiency with which matter accretes in the propeller regime (Romanova et al. 2004); some X-ray binaries believed to be accreting in the propeller regime nevertheless show X-ray emission from accretion (e.g. Gungor et al. 2017). We assume that growth of the NS mass occurs at the rate

$$\frac{dM_{\text{ns}}}{dt} = \begin{cases} \dot{M}, & \dot{M} \gtrsim \dot{M}_c \\ f_{\text{acc}}\dot{M} & \dot{M} \lesssim \dot{M}_c \end{cases}, \quad (19)$$

where $f_{\text{acc}} < 1$ is the accretion efficiency in the propeller regime. Though we adopt $f_{\text{acc}} = 0$ in what follows, this is easily generalizable and our main conclusions are not sensitive to this assumption.

An accreting magnetar can reach a approximate equilibrium for which $dJ/dt \approx 0$, either exactly or in a time-averaged sense, depending on the adopted prescription for angular momentum loss in the propeller regime, $n(\omega)$. Accretion spin-up ($\dot{J}_{\text{acc}} > 0$) can be balanced either by wind spin-down ($\dot{J}_{\text{sd}} = \dot{E}_{\text{sd}}/\Omega < 1$) or propeller spin-down ($\dot{J}_{\text{acc}} < 0$; in the Piro & Ott 2011 prescription). This equilibrium occurs for $\omega \approx 1$, corresponding to a spin period of

$$P_{\text{eq}} = P_c \simeq 1.52 B_{15}^{6/7} \dot{M}_{-2}^{-3/7} M_{1.4}^{-5/7} \text{ms}. \quad (20)$$

The timescale needed to maintain equilibrium can be estimated as

$$\tau_{\text{eq}} \equiv \frac{I\Omega_{\text{eq}}}{\dot{M}(GM_{\text{ns}}R_m)^{1/2}} \approx 13.2 B_{15}^{-8/7} \dot{M}_{-2}^{-3/7} M_{1.4}^{16/7} \text{s}, \quad (21)$$

where $\Omega_{\text{eq}} = 2\pi/P_{\text{eq}}$.

This equilibrium is in some sense more “robust” for the Piro & Ott (2011) coupling prescription, because if ω becomes $\gtrsim 1$, then the disk torque becomes negative (propeller spin-down), driving ω back to $\simeq 1$. As long as the mass accretion rate evolves relatively slowly compared to τ_{eq} then $P \approx P_{\text{eq}}$ will be maintained.

Though a similar equilibrium condition (20) may be achieved also for the Parfrey et al. (2016) prescription (eq. 18), in this case if ω evolves to become $\gtrsim 1$ then the disk no longer exerts a torque on the star. As long as the accretion rate evolves slowly, then spin-down of the star will drive $\omega \lesssim 1$ again, temporarily restoring $\omega \approx 1$ and resulting in a time-average equilibrium with $P \approx P_{\text{eq}}$. However, if instead the accretion rate decreases rapidly compared to the spin-down time of the isolated magnetar (i.e. $t_{\text{fb}} \ll t_{\text{sd},3}$), then the star can decouple permanently from the disk and spin-down will proceed independently of an subsequent mass fall-back.

3. RESULTS

3.1. Spin-Down Evolution

We solve equations (11), (19) for the evolution of the magnetar spin period $P(t)$ and the spin-down power

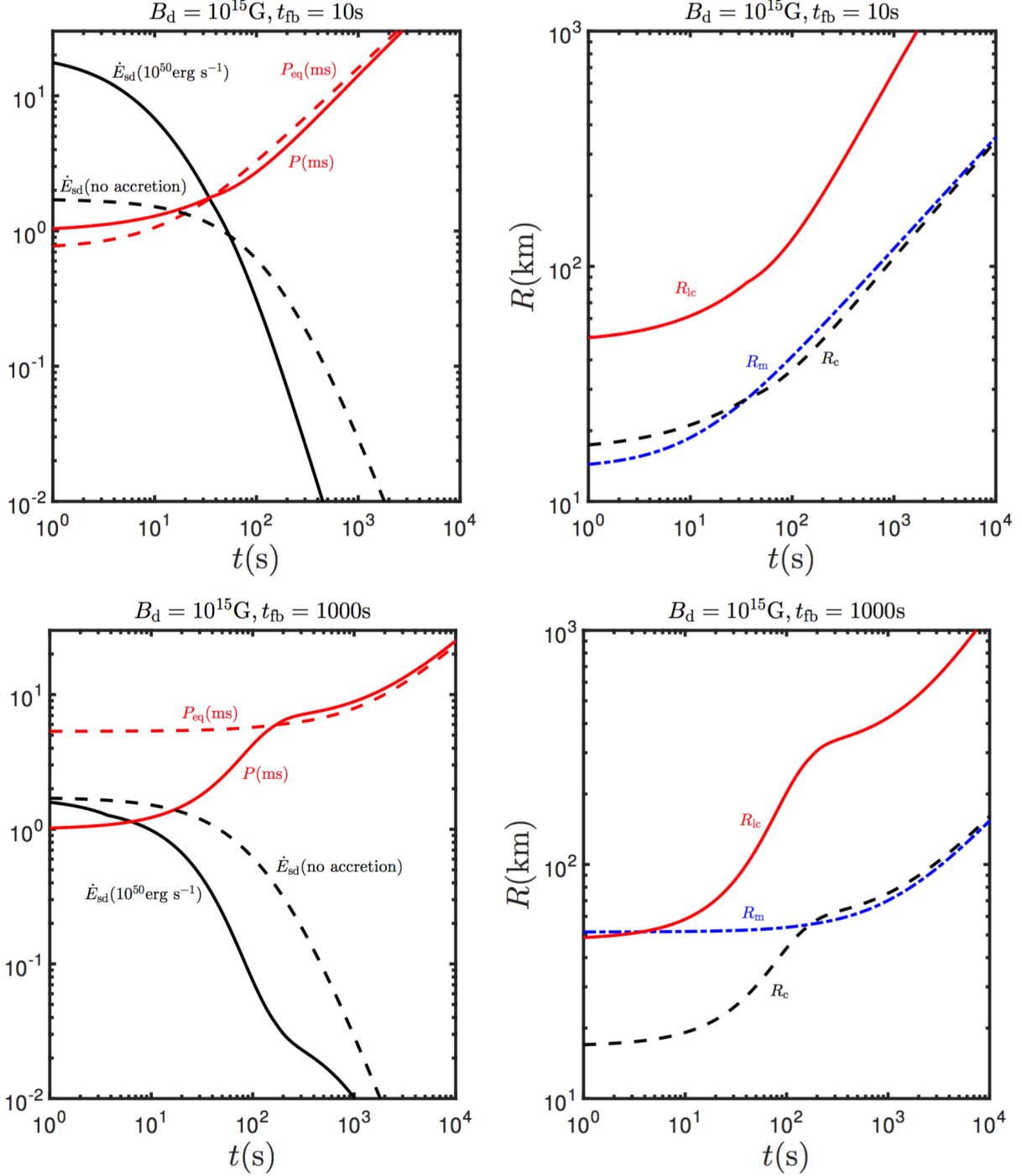


FIG. 3.— Spin down evolution of an accreting magnetar with surface dipole field strength of $B_d = 10^{15}$ G and initial spin period $P_0 = 1$ ms, assuming mass fall-back with $M_{fb} = 0.8M_\odot$ over a timescale $t_{fb} = 10$ s (top panels) and $t_{fb} = 10^3$ s (bottom panels). The left panels show the spin-down luminosity \dot{E}_{sd} (black solid curve), compared to its equivalent evolution without fall-back accretion (black dashed curve). Also shown is the magnetar spin period P (solid red curve) compared to its value in equilibrium $P_{eq} = P_c$ (dashed red curve) at which $R_m \approx R_c$ (eq. 20). The right panels show several critical radii: light cylinder R_{lc} (solid red curve), Alfvén R_m (dotted blue curve), and co-rotation R_c (dashed black curve). These models are calculated using the Piro & Ott (2011) prescription for the \dot{J} coupling between the accretion disk and NS magnetosphere (eq. 17).

$\dot{E}_{sd}(t)$ given the initial properties of the magnetar (B_d , birth spin period P_0) and the externally imposed mass fall-back evolution $\dot{M}(t)$ (eq. 1). Because we are interested in exploring the maximal effects of accretion, we fix the total fall-back mass at the maximum value $M_{fb} = 0.8M_\odot$ needed to avoid gravitational collapse to

a black hole and explore the dependence of the result on the fall-back time, t_{fb} .

Figure 3 shows two examples of $\dot{E}_{sd}(t)$ and $P(t)$ for $B_d = 10^{15}$ G, $P_0 = 1$ ms, $f_{acc} = 0$, for different values of the mass fall-back time $t_{fb} = 10$ s (top panel) and $t_{fb} = 10^3$ s (bottom panel), employing the Piro

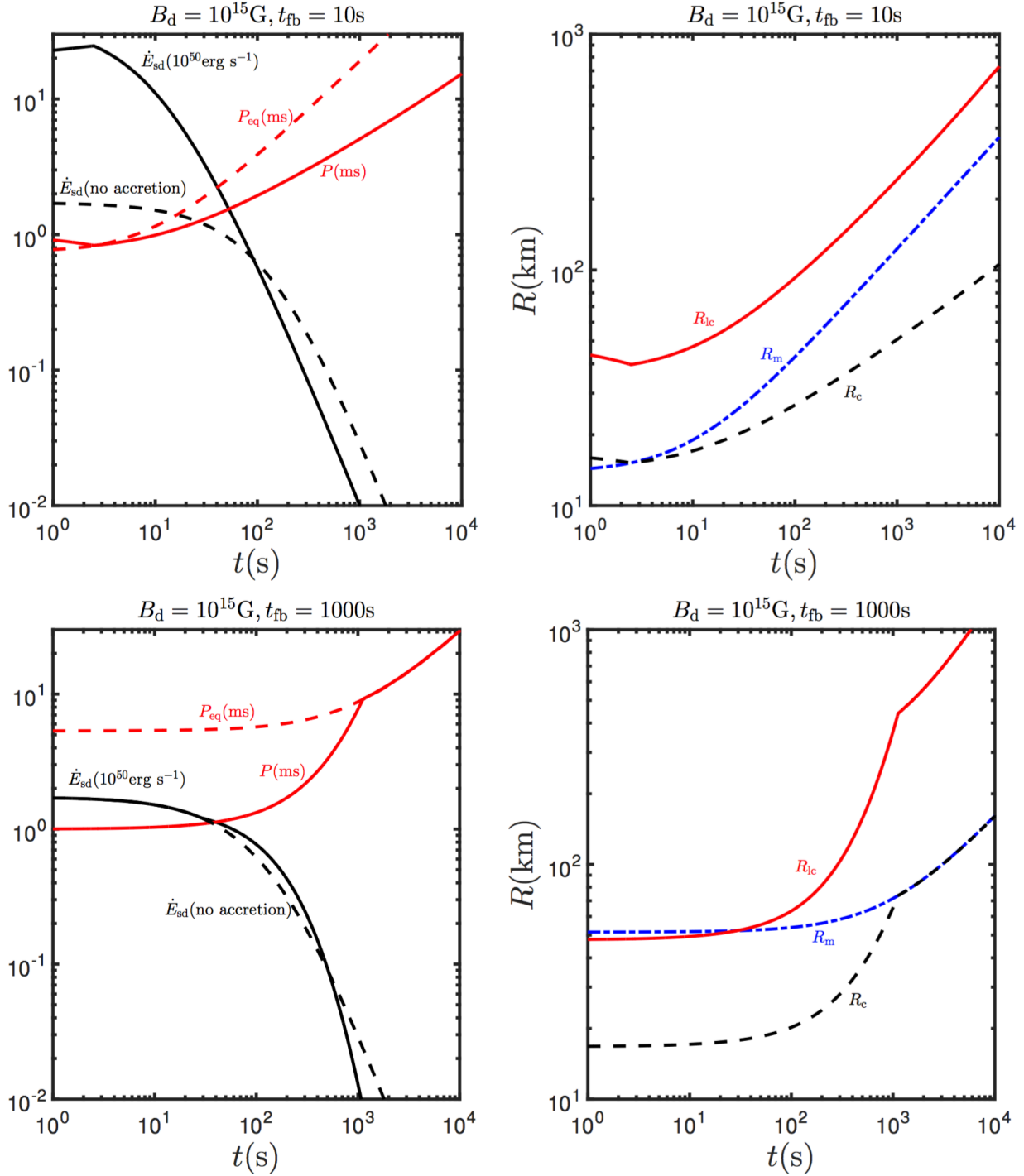


FIG. 4.— Same as Fig. 3, but assuming zero \dot{J} coupling between the accretion disk and the NS magnetosphere in the propeller regime (Parfrey et al. 2016; eq. 18).

& Ott (2011) disk-magnetosphere coupling prescription (eq. 17). In both cases the spin period achieves the equilibrium value P_{eq} (eq. 20), but the effects on \dot{E}_{sd} are markedly different. In the high \dot{M} case ($t_{\text{fb}} = 10 \text{ s}$), the initial value of \dot{E}_{sd} exceeds by an order of magnitude the otherwise equivalent case of a non-accreting magnetar (shown for comparison with a black dashed curve) as a result of the enhanced spin-down caused by $R_{\text{m}} < R_{\text{lc}}$.

In the low \dot{M} case ($t_{\text{fb}} = 10^3 \text{ s}$), the spin equilibrium

$P = P_{\text{eq}}$ is also rapidly achieved on a timescale $\sim 0.1 t_{\text{fb}}$. However, the evolution starts with $R_{\text{m}} \approx R_{\text{lc}} \gg R_{\text{c}}$, such that, although the initial spin-down luminosity is similar to the isolated magnetar case, angular momentum losses in the propeller regime reduce the total rotational energy which is extracted by the magnetar wind to $\int \dot{E}_{\text{sd}} dt \approx 10^{52} \text{ erg}$, less than half the value for an otherwise equivalent isolated magnetar with the same birth period.

If the equilibrium $P = P_{\text{eq}}$ (eq. 20) is achieved, then

the luminosity of the magnetar wind evolves as

$$\begin{aligned} \dot{E}_{\text{sd,eq}} &\simeq \frac{\mu^2 \Omega^4}{c^3} \frac{R_{\text{lc}}^2}{R_c^2} \Big|_{P=P_{\text{eq}}} \\ &\simeq 3.44 \times 10^{50} B_{15}^{-6/7} \dot{M}_{-2}^{10/7} M_{1.4}^{12/7} \text{ ergs s}^{-1}. \end{aligned} \quad (22)$$

Taking $\dot{M} = 0.8 M_\odot / t_{\text{fb}}$, the timescale to reach spin equilibrium (eq. 21) relative to the fall-back time is given by

$$\frac{\tau_{\text{eq}}}{t_{\text{fb}}} \approx 0.54 B_{15}^{-8/7} (t_{\text{fb}}/10 \text{ s})^{-4/7} M_{1.4}^{16/7}, \quad (23)$$

while relative to the spin-down time we have

$$\frac{\tau_{\text{eq}}}{t_{\text{sd},2}} \approx 0.55 B_{15}^{-2/7} (t_{\text{fb}}/10 \text{ s})^{-1/7} M_{1.4}^{1/2}. \quad (24)$$

For the parameter ranges of interest we have $\tau_{\text{eq}} \ll t_{\text{fb}}, t_{\text{sd},2}$, indicating that equilibrium will be achieved over timescales relevant to the system evolution. Furthermore, if $\dot{M} \propto t^{-5/3}$ then $\tau_{\text{eq}}/t \propto t^{-2/7}$ at times $t \gg t_{\text{fb}}$, such that an equilibrium which is achieved by $t \sim t_{\text{fb}}$ will be maintained at all later times despite the declining accretion rate.

If the late-time accretion rate decreases as $\dot{M} \propto t^{-\zeta}$, then the outflow power will approach a power-law decay

$$\dot{E}_{\text{sd}} \propto \dot{M}^{10/3} \propto t^{-10\zeta/3} = \begin{cases} t^{-2.38}, & \zeta = 5/3, \\ t^{-1.90}, & \zeta = 4/3. \end{cases} \quad (25)$$

This decay can be steeper or shallower than the standard $\dot{E}_{\text{sd}} \propto t^{-2}$ prediction for isolated dipole spin-down, depending on whether the mass accretion rate is dominated by the mass fall-back rate ($\zeta = 5/3$) or a viscously-spreading disk ($\zeta = 4/3$). Also note that this late-time evolution will persist only until the co-rotation radius $R_c \propto P^{2/3}$ grows to exceed the circularization radius or the outer edge of the viscously-expanding accretion disk.

Figure 4 shows for comparison an otherwise identical calculation which instead employs the minimal Parfrey et al. (2016) disk-magnetosphere coupling (eq. 18). The main qualitative difference, as compared to the case employing the Piro & Ott (2011) prescription, is that the equilibrium condition $R_m \approx R_c (\omega \approx 1)$ no longer necessarily obtains. If the system begins in the propeller regime ($R_m > R_c$; $\omega \gtrsim 1$), then whether $\omega \approx 1$ is achieved depends on the timescale over which the mass fall-back rate declines relative to the spin-down time, $t_{\text{sd},3}$. For the Parfrey et al. (2016) prescription, $\dot{J}_{\text{acc}} = 0$ for $\omega > 1$ and spin-down occurs exclusively due to the magnetar wind. If $t_{\text{fb}} \ll t_{\text{sd},3}$ (as in the example shown in the top panel of Fig. 4), then R_m increases $\propto t^{10/21}$ while R_c grows more slowly in time, such that $\omega > 1$ is maintained and no equilibrium is achieved. By contrast, if $t_{\text{fb}} \gg t_{\text{sd},3}$ (and/or if $\omega < 1$ initially), then the $\omega \approx 1$ condition is achieved, as in the example shown in the bottom panel of Fig. 4.

Figure 5 shows contours of the total extracted energy $E = \int \dot{E}_{\text{sd}} dt$ from the magnetar wind as a function of B_d and P_0 for two values of the fall-back time, $t_{\text{fb}} = 10$ s (left panel) and $t_{\text{fb}} = 10^5$ s (right panel), and adopting the Piro & Ott (2011) coupling. These two cases approximately cover the parameter space relevant to magnetars powering long GRBs and SLSNe, respectively. Shown for

comparison with horizontal lines are the total rotational energy of non-accreting magnetars with the same initial spin period, $E_{\text{rot}}(P_0)$ (eq. 10).

For relatively weak magnetic fields B_d and slow rotation $P_0 \gtrsim$ few ms, spin-up from accretion increases the extracted rotational energy as compared to an otherwise equivalent non-accreting case. This has the important implication that the range of magnetar properties capable of producing GRBs or SLSNe is greatly enhanced by the effects of accretion. On the other hand, for large B_d and small P_0 , accretion can act to decrease the effective rotational energy reservoir of the magnetar wind via the propeller mechanism. Across most of the parameter space, \dot{E} does not greatly exceed the maximum initial rotational period $E_{\text{rot}}(P_0) \approx \text{few} \times 10^{52}$ ergs for an isolated magnetar rotating near break-up.

We further illustrate the latter point by analytically estimating the maximum rotational energy which can be extracted from a magnetar under the constraint that the total accreted mass be $M_{\text{acc}} \lesssim 0.8 M_\odot$. For $\dot{M} \lesssim \dot{M}_c$ accretion either removes angular momentum from the magnetar or has no effect on its spin-down evolution as compared to the non-accreting case. For $\dot{M} \gtrsim \dot{M}_c$ the magnetar gains angular momentum and quickly approaches the equilibrium state $\dot{M} \simeq \dot{M}_c$ ($P = P_{\text{eq}}$) for which the wind luminosity obeys $\dot{E}_{\text{sd}} = \dot{E}_{\text{sd,eq}}$ (eq. 22). Substituting $\dot{M} = 0.8 M_\odot / \Delta t$, the extracted rotational energy in a time interval Δt is

$$E = \dot{E}_{\text{sd,eq}} \Delta t = 6.7 \times 10^{52} B_{15}^{-6/7} (\Delta t/10 \text{ s})^{-3/10} M_{1.4}^{12/7} \text{ ergs}. \quad (26)$$

The shortest allowed value of $(\Delta t)_{\text{min}} = 9.3 \text{ s } B_{15}^{-2} M_{1.4}^{1/2}$ (largest E) is set by the requirement that $\dot{M} = \dot{M}_{\text{ns}}$, since for $\dot{M} \gtrsim \dot{M}_{\text{ns}}$ the spin-down rate no longer increases with increasing \dot{M} . Thus, we have a maximum extractable energy

$$E_{\text{max}} = \dot{E}_{\text{sd,eq}} (\Delta t)_{\text{min}} = 6.7 \times 10^{52} B_{15}^{-0.26} M_{1.4}^{1.56} \text{ ergs}, \quad (27)$$

which is less than a few times higher than the maximum initial rotational energy. Equation 27 should also be augmented to include the remaining rotational energy after the accretion subsides, which, though comparable to E_{max} , will emerge over longer timescales due to the slower spin-down of a non-accreting magnetar.

3.2. ^{56}Ni Production in GRB Supernovae

In order to explain the large masses $\gtrsim 0.2 - 0.3 M_\odot$ of radioactive ^{56}Ni needed to power the light curves of GRB SNe (e.g. Mazzali et al. 2014) by shock-heating the inner layers of the progenitor star, the central engine outflow must inject $E \sim 10^{52}$ ergs of energy on a short timescale of $\lesssim 1$ s following the explosion (e.g. Barnes et al. 2017). Without accretion-induced enhancement of the spin-down power, this would require a magnetar with a short initial spin period $P_0 \sim 1$ ms and a very strong magnetic field $B_d \gtrsim 10^{16}$ G in order to obtain a spin-down time $t_{\text{sd},3}$ of less than a few seconds (Suwa & Tominaga 2015). However, such a magnetar would spin-down quickly, sapping the rotational energy needed to power the GRB jet at later times (§3.3).

On the other hand, when the accretion enhancement of

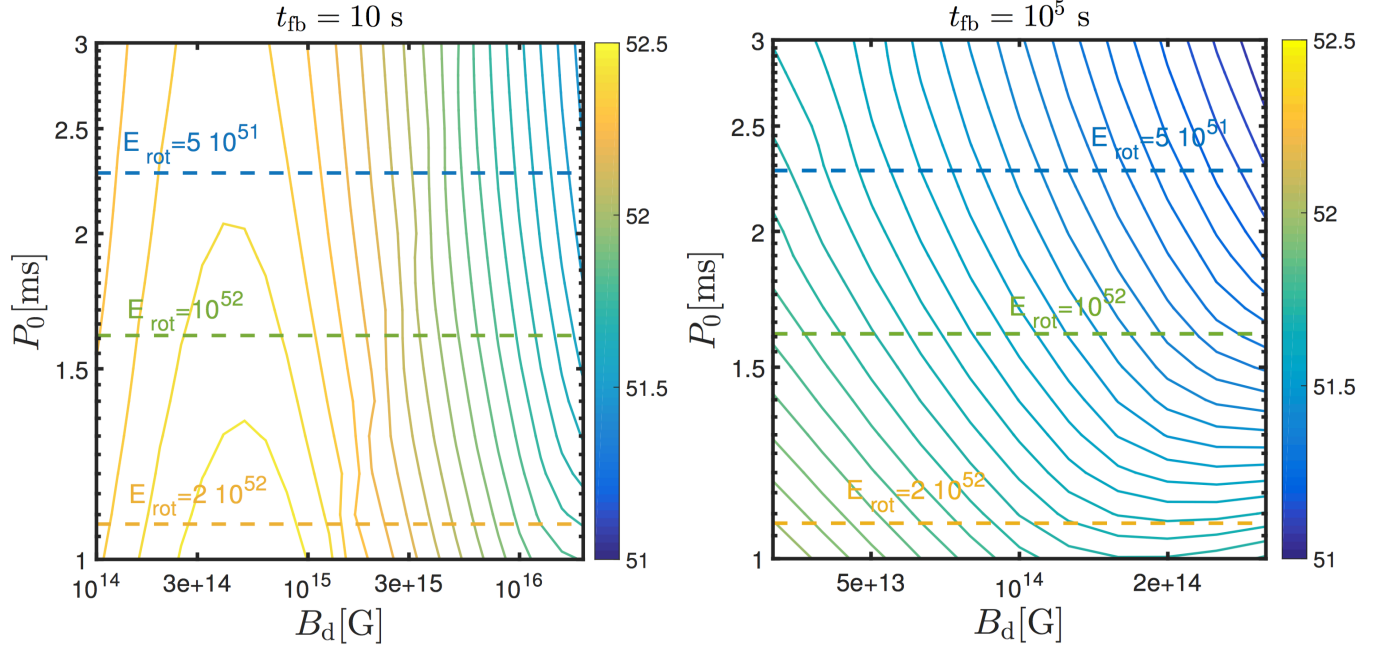


FIG. 5.— Total rotational energy $E = \int \dot{E}_{\text{sd}} dt$ extracted in the magnetized wind of a proto-magnetar of initial mass $M_{\text{ns}} = 1.4M_{\odot}$ as a function of its dipole field strength B_d and birth spin period P_0 , accounting for the effects of mass fall-back of total quantity $M_{\text{fb}} = 0.8M_{\odot}$ over a timescale $t_{\text{fb}} = 10$ s (left panel) and $t_{\text{fb}} = 10^5$ s (right panel). The range of $(B_d, P_0, t_{\text{fb}})$ covered in the two cases correspond to parameters appropriate for magnetars capable of powering long GRB jets and SLSNe, respectively. The total rotational energy of non-accreting magnetars with the same initial spin period are shown for comparison with dashed lines.

the spin-down rate is taken into account, from equation (12) we see that for $P \sim 1$ ms a magnetic field $B_d \gtrsim 2 \times 10^{15}$ G is sufficient for a jet power $\dot{E}_{\text{sd}} \gtrsim 10^{52}$ ergs s^{-1} , provided the accretion rate is close to the monopole spin-down limit, $\dot{M} \gtrsim \dot{M}_{\text{ns}} \approx 0.086 B_{15}^2 M_{1.4}^{-1/2} M_{\odot} \text{ s}^{-1}$. Even at such a high accretion rate, the total mass accreted by the magnetar of $\sim 0.1M_{\odot}$ over the necessary timescale ~ 1 s would be insufficient to instigate its collapse to a black hole.

To illustrate this point, Fig. 6 considers a hypothetical mass accretion history characterized by two separate fall-back episodes. The first episode has $t_{\text{fb}} \approx 0.1$ s and carries a mass $M_{\text{fb}} \approx 0.5M_{\odot}$, while the second component has $M_{\text{fb}} \approx 0.3M_{\odot}$ and $t_{\text{fb}} \approx 5$ s. As shown in the left panel of Fig. 6, the jet power reaches values of $\dot{E}_{\text{sd}} \approx 10^{52}$ ergs s^{-1} on timescales of $t \lesssim 0.5$ s, while remaining $\gtrsim 3 \times 10^{50}$ ergs s^{-1} at $t \gtrsim 10$ s. Such a jet evolutionary history can account for the large ^{56}Ni masses of GRB-SNe, while also producing a GRB jet of sufficient power over longer timescales. Assuming that the spin-down energy released when the magnetization of the outflow obeys $100 \leq \sigma \leq 3000$ goes into powering the GRB jet (see §3.3), while the remainder goes into feeding the kinetic energy of the SN explosion, we find total energies of the SN and GRB components of $E_{\text{SN}} \approx 2 \times 10^{52}$ ergs and $E_{\text{GRB}} \approx 3 \times 10^{51}$ ergs, respectively; 90% of the later is released within a time $\lesssim 70$ s, typical of a long GRB duration.

3.3. GRB Jet Evolution

The wind from the magnetar is a promising source for feeding the relativistic GRB jet (Thompson et al. 2004), which escapes from the stellar ejecta on timescales of $\gtrsim 5$ – 10 s in the case of normal long GRBs (e.g. Bromberg

et al. 2011; Aloy et al. 2018).⁶ Once a successful jet is established through the star, non-axisymmetric instabilities within the jet appear to have only a relatively weak impact on its structure (Bromberg & Tchekhovskoy 2016) and a large fraction of the power carried by the magnetar wind will be placed into the luminosity of the jet, $L_j = \dot{E}_{\text{sd}}$ (Bucciantini et al. 2009).

A key property of the jet is its magnetization, or maximum attainable bulk Lorentz factor, given by

$$\sigma = \frac{L_j}{\dot{M}_j c^2}, \quad (28)$$

where \dot{M}_j is the rate at which baryon mass leaves the NS surface along the open magnetic flux (the red region in Fig. 2).

For a weakly-magnetized NS, the neutrino wind is approximately spherical in geometry, and the mass loss rate due to neutrino ablation is approximately parameterized by (Metzger et al. 2011)

$$\dot{M}_{\nu,0}(t) = 3 \times 10^{-4} (1 + t/t_{\text{kh}})^{-5/2} e^{-t/t_{\text{thin}}} M_{\odot} \text{ s}^{-1}, \quad (29)$$

where $t_{\text{kh}} \approx 2$ s is the Kelvin-Helmholtz cooling timescale of the proto-NS and we have assumed a NS cooling evolution appropriate for a NS of mass $M_{\text{ns}} = 2M_{\odot}$ (Pons et al. 1999; see Metzger et al. 2011 for details). Absent the effects of accretion, the mass loss rate cuts off abruptly after the NS becomes optically thin to neutrinos, on a timescale of $t_{\text{thin}} \approx 10$ – 30 s; hereafter we take $t_{\text{thin}} = 20$ s.

⁶ The timescale for jet escape is shorter in the case of NS mergers due to the small ejecta mass (e.g. Bucciantini et al. 2012; Bromberg et al. 2017) but longer in ultra-long GRBs due to the lower jet luminosity and/or more radially-extended progenitor star (Quataert & Kasen 2012; Margalit et al. 2018).

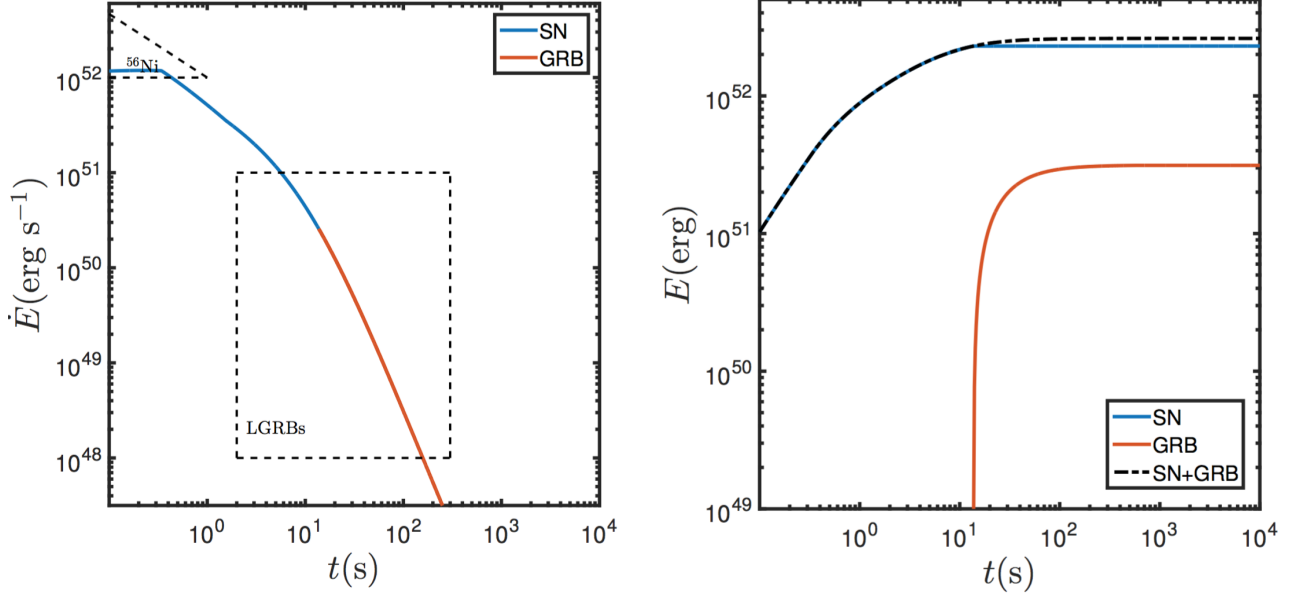


FIG. 6.— The magnetar wind can both power the supernova (by contributing to its kinetic energy and by shock-heating the inner layers of the star to produce sufficient ^{56}Ni) as well as the subsequent GRB jet. Here we show a magnetar with $B_d = 2 \times 10^{15}$ G and $P_0 = 1$ ms that experiences a hypothetical two-component fall-back history comprised of separate accretion episodes with $t_{\text{fb},1} \approx 0.1$ s, $M_{\text{fb},1} \approx 0.5 M_\odot$ and $t_{\text{fb},2} \approx 5$ s, $M_{\text{fb},2} \approx 0.3 M_\odot$, respectively, where each component follows the temporal form given by equation (1). Energy released when the magnetization of the magnetar outflow is in the range $100 \leq \sigma \leq 3000$ contributes to the GRB jet (red curves; see §3.3), while at earlier times when $\sigma \leq 100$ the wind contributes to powering the SN (blue curves). As shown in the left panel, the jet power is $\dot{E}_{\text{sd}} \approx 10^{52}$ ergs s^{-1} in the first $\lesssim 0.5$ s, sufficient to produce the requisite large quantity of ^{56}Ni by shock-heating the inner layers of the supernova ejecta (e.g. [Suwa & Tominaga 2015](#); [Barnes et al. 2017](#)), yet the jet power remains $\gtrsim 3 \times 10^{50}$ ergs s^{-1} for a timescale ~ 10 s typical of the duration of a long GRB. The right panel shows the cumulative energy released in the SN and GRB components, which total to $E_{\text{SN}} = 2 \times 10^{52}$ ergs and $E_{\text{GRB}} = 3 \times 10^{51}$ ergs, respectively.

Accretion introduces an additional source of neutrino-driven mass loss from the neutrinos produced as matter settles onto the NS from the magnetic accretion column ([Piro & Ott 2011](#)). This additional neutrino luminosity $L_{\nu,\text{acc}} \approx GM_{\text{ns}}\dot{M}/R_{\text{ns}}$ will irradiate the polar cap (e.g. [Zhang & Dai 2010](#)), where the outflow is being driven outwards along the open field lines (Fig. 2). This contributes an additional mass loss rate of

$$\dot{M}_{\nu,\text{acc}} = 1.2 \times 10^{-5} M_{1.4} \dot{M}_{-2}^{5/3} M_\odot \text{s}^{-1}, \quad (30)$$

which decays on the fall-back time-scale t_{fb} instead of t_{thin} ; thus $\dot{M}_{\nu,\text{acc}}$ always exceeds $\dot{M}_{\nu,0}$ at sufficiently late times.

Above the magnetar surface, magnetic pressure greatly exceeds the thermal pressure from neutrino heating (e.g. [Thompson et al. 2004](#); [Vlasov et al. 2014](#)). Thus, only the fraction f_Φ of the magnetar surface threaded by open magnetic flux is open to mass outflow (however, see [Thompson 2003](#); [Thompson & ud-Doula 2017](#)). The baryon loading is thus suppressed relative to the case of a weakly-magnetized wind by a factor

$$\frac{\dot{M}_j}{\dot{M}_\nu} = f_\Phi f_{\text{cent}} \approx \begin{cases} 0.5 f_{\text{cent}} & \dot{M} \gtrsim \dot{M}_{\text{ns}} \\ \frac{R_{\text{ns}}}{2R_m} \approx 0.27 f_{\text{cent}} B_{15}^{-4/7} \dot{M}_{-2}^{2/7} M_{1.4}^{1/7} \dot{M}_{\text{lc}} \lesssim \dot{M} \lesssim \dot{M}_{\text{ns}} & \dot{M} \gtrsim \dot{M}_{\text{ns}} \\ \frac{R_{\text{ns}}}{2R_{\text{lc}}} \approx 0.13 f_{\text{cent}} P_{\text{ms}}^{-1} & \dot{M} \lesssim \dot{M}_{\text{lc}}, \end{cases} \quad (31)$$

where $\dot{M}_\nu = \dot{M}_{\nu,0} + \dot{M}_{\nu,\text{acc}}$ and we have taken $f_\Phi = 0.5$ for $R_m = R_{\text{ns}}$ to account for the fact that the

geometrically-thick accretion disk covers roughly half of the NS surface in this limit. Here

$$f_{\text{cent}} = \exp[(P_c/P)^{1.5}]; \quad P_c \simeq 2.7 \sin \theta_{\text{lc}} M_{1.4}^{-1/2} \text{ ms} \quad (32)$$

accounts for the enhancement to the mass-loss rate due to centrifugal forces in proto-NS atmosphere ([Metzger et al. 2007](#)), where again $\theta_{\text{lc}} = \sin^{-1}(R_{\text{ns}}/R_m)^{1/2}$ is the polar latitude of the last closed field line; the distance measured from the rotation axis to this location on the NS surface defines the centrifugal “lever arm” at the base of the wind where most of the mass flux emerges.

Figure 7 shows the evolution of the jet power and magnetization as a function of time for a magnetar with $B_d = 10^{15}$ G, $P_0 = 1$ ms which accretes $0.8 M_\odot$ in fall-back over a timescale $t_{\text{fb}} = 3$ s (left panel) and $t_{\text{fb}} = 300$ s (right panel). In addition to the enhancement of the spin-down rate discussed earlier, the additional baryon-loading of the jet due to accretion causes the jet magnetization to rise much slower at late times as compared to the isolated (non-accreting) case.

GRB prompt emission models typically require high but not excessive magnetization. Since σ is an upper limit on the terminal Lorentz factor of the jet, Γ , compactness arguments impose a strong limit of $\sigma \geq \Gamma \gtrsim 100$ ([Fenimore et al. 1993](#); [Woods & Loeb 1995](#); [Lithwick & Sari 2001](#)). In many dissipation models σ is in fact expected to be comparable to Γ . The latter is estimated from peaks in GRB afterglows and found to reside in the range $100 \lesssim \Gamma \lesssim 3000$ ([Liang et al. 2010](#); [Lü et al. 2012](#); [Ghirlanda et al. 2012](#)). In models based on gradual magnetic reconnection, the same range of Γ, σ is also required from a purely theoretical perspective ([Beniamini](#)

& Giannios 2017).

Because of this restricted ‘useful’ range in σ , the more gradual rise in σ from an accreting magnetar acts to significantly extend the duration of the prompt emission phase. Without fall-back accretion, the timescale t_σ over which the magnetization obeys $10^2 \lesssim \sigma \lesssim 3000$ is limited to $t_\sigma \lesssim \text{few} \times t_{\text{thin}} \lesssim \text{tens of seconds}$. However, when the effects of accretion are included, t_σ can be significantly lengthened; for the example shown in the right panel of Fig. 7, t_σ increases from ≈ 5 s for $\dot{M} = 0$ to ≈ 5000 s with accretion present.

Figure 8 shows $T_{\text{GRB}} = \min(t_\sigma, t_{\text{sd}})$, a proxy for the GRB duration, in the parameter space of B_d and P_0 , taking into account the effects of fallback accretion. This definition accounts for the fact that t_σ only controls the duration of the GRB prompt emission when it does not exceed the spin-down timescale of the magnetar, t_{sd} . Shown for comparison with dashed lines are the predicted GRB durations without accretion. When the effects of accretion are included, the GRB duration for $B_d \sim 10^{14} - 10^{15}$ G is increased by $\gtrsim 1 - 2$ orders of magnitude as compared to the non-accreting case. This finding has the implication that the magnetar model can accommodate ultra-long GRBs with prompt emission that lasts for a duration $T_{\text{GRB}} \sim 10^3 - 10^4$ s (e.g. Greiner et al. 2014; Levan 2015). Since the spectral energy distribution of the GRB depends in most models on the jet magnetization, accretion acts to reduce the predicted rate of spectral evolution during the burst. This places the magnetar model in more comfortable agreement with time-resolved observations of GRB spectra, which generally show at most moderate hard-to-soft evolution (e.g. Kargatis et al. 1994).

An upper limit on the prompt GRB energy is given by E_σ , the total rotational energy extracted from the magnetar as the wind evolves from $\sigma = 100$ to $\sigma = 3000$ (Beniamini et al. 2017), as shown in Figure 9. As in the case of the total extracted rotational energy, we find that $E_\sigma \lesssim 10^{52}$ ergs across the parameter space of surface magnetic field and initial spin period. Thus, even when including the effects of fall-back accretion, the total available energy for the GRB phase is limited to values similar to the isolated magnetar case.

3.4. GRB with Long Precursor Gaps

While the magnetization of the jet powered by an isolated, non-accreting magnetar rises monotonically (e.g. Metzger et al. 2011), the evolution of $\sigma(t)$ when the effects of accretion are included (§3.3) can be substantially more complex and even non-monotonic, depending on the relative ordering of the timescales t_{fb} , t_{kh} , t_{thin} , t_{eq} . For $B_d \gtrsim 7 \times 10^{15}$ G, the value of σ reaches high values at early times ≥ 100 , before decreasing to values $\sigma \approx 30$ over the next few seconds as the magnetar quickly spins down due to accretion, before eventually rising up again to large values $\sigma \gtrsim 100$ as the magnetar cools and the neutrino-driven baryon loading of the jet subsides. If the jet magnetization must be in the critical range $100 \leq \sigma \leq 3000$ in order to produce prompt gamma-ray emission, then this complex σ evolution would imprint an equally complex GRB light curve. One would expect ‘precursor’ emission during the brief early high- σ phase, followed by an extended gap without prompt emission

when σ is low, which is then finally accompanied by a second GRB emission episode as σ again rises at late times.

Figure 10 provides an explicit example of this behavior for a magnetar with $B_d = 10^{16}$ G and $P_0 = 1$ ms that accretes $0.8M_\odot$ over a time $t_{\text{fb}} = 1000$ s. In this case the precursor phase lasts for 1.5 s and releases 7.8×10^{51} ergs. This is then followed by a ≈ 40 s gap, after which a second GRB phase commences, which releases an additional 6×10^{50} ergs over a duration of $\sim 10^4$ s. Although future work is needed to determine whether such a scenario can reproduce observed GRB precursors in detail, the jet evolution of an accreting magnetar is clearly substantially more complex than from an isolated one, helping to explain the wide diversity in GRB light curves.

3.5. Binary NS Mergers

The merger of two NSs in a binary can result in the formation of a massive NS remnant, which is at least temporarily stable to gravitational collapse due to its rapid rotation (Metzger et al. 2008b; Bucciantini et al. 2012; Rowlinson et al. 2013; Giacomazzo & Perna 2013; Zhang 2013; Gao et al. 2015). As a result of the large orbital angular momentum of the initial binary, the remnant is rotating at close to its centrifugal break-up limit of $P_0 \lesssim 1$ ms and will possess a strong magnetic field, at least on small spatial scales (e.g. Price & Rosswog 2006).

As in the core collapse case, such a magnetar remnant will accrete matter over an extended period after the merger, as marginally-bound high angular-momentum material falls back into a disk surrounding the merger and the remnant disk feeds matter onto the NS (Rosswog 2007; Metzger et al. 2009, 2010; Fernández & Metzger 2013; Metzger & Fernández 2014; Fernández et al. 2017). The total accreted mass is typically in the range $M_{\text{acc}} \sim 0.01 - 0.1M_\odot$ and the peak accretion rate is $\sim 0.1 - 1M_\odot \text{ s}^{-1}$, where the characteristic ‘fall-back’ time $t_{\text{fb}} \sim 0.1$ s may in this case be controlled by the viscous timescale of the torus.

For $P \simeq 0.8$ ms and $M = 2.4M_\odot$, we see that $\dot{M}_{\text{ns}} \simeq 4\dot{M}_c \approx 0.07B_{15}^2 M_\odot \text{ s}^{-1}$. Therefore, unless $B_d \gg 10^{15}$ G, the accretion rate is sufficiently high at early times to push the Alfvén radius down by the disk to the NS surface. For $t_{\text{fb}} = 0.1$ s, and magnetic field strength of $B_d = 3 \times 10^{14} - 3 \times 10^{15}$ G, we find that if the magnetar remnant is indefinitely stable (i.e. does not collapse to a black hole during its spin-down), then the total energy extracted in the magnetar wind is $\approx 1 - 2 \times 10^{52}$ ergs (adopting the Piro & Ott 2011 prescription), somewhat lower than the rotational energy 8×10^{52} ergs which would be available were the magnetar spinning-down in isolation. Eventually, as \dot{M} continues to decrease an equilibrium will be established with $R_m \simeq R_c$ (as in the core collapse case), such that the spin-down luminosity will approach the decay $\dot{E}_{\text{sd}} \propto t^{-1.9}$ (eq. 25); however, in practice the time required to achieve this equilibrium is long, $\sim 3 \times 10^3 - 3 \times 10^6$ s, depending on B_d . Gompertz et al. (2014) and Gibson et al. (2017) explore a related model for the propeller-driven outflows from accreting magnetars as an explanation for the temporally-extended X-ray emission observed after some short GRBs.

Instead of an indefinitely stable NS that spins down

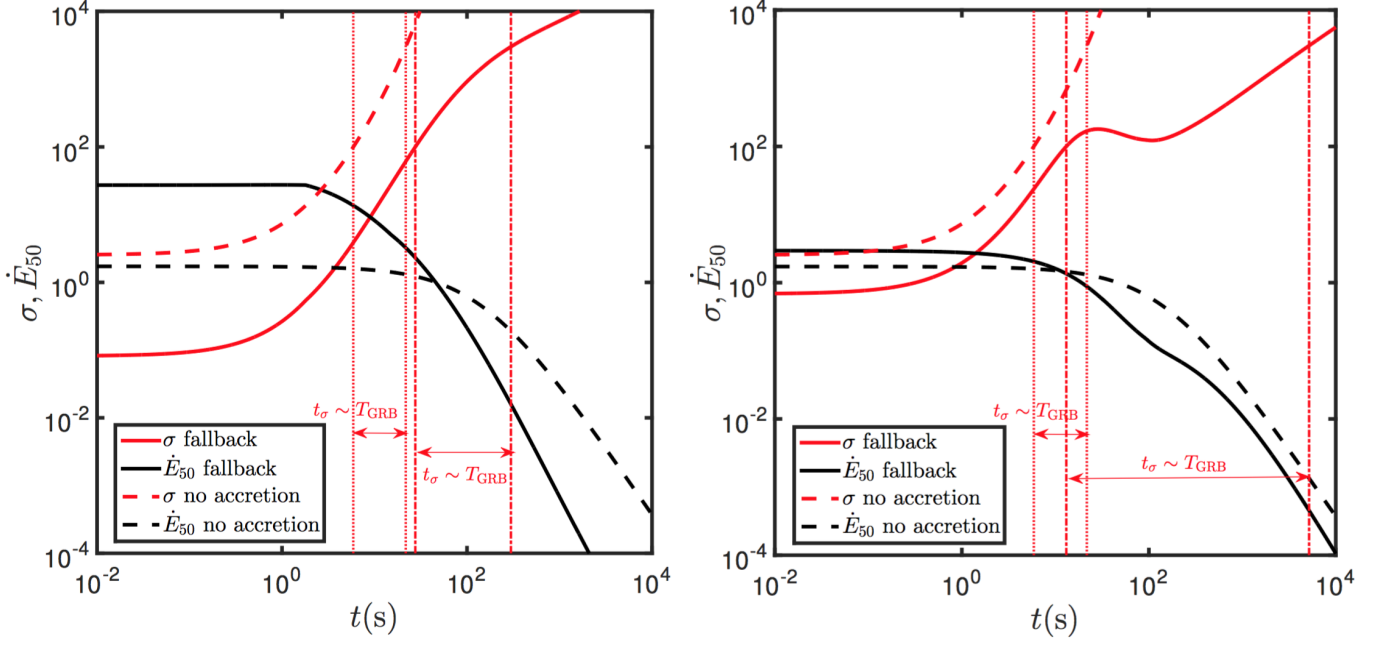


FIG. 7.— The additional baryon-loading from fall-back accretion can appreciably lengthen the duration of the prompt GRB emission. This figure shows the jet power $L_j(t) = \dot{E}_{\text{sd}}$ (in units of $10^{50} \text{ ergs s}^{-1}$; black curve) and magnetization $\sigma(t)$ (red curve) for a magnetar with $B_d = 10^{15} \text{ G}$ and an initial spin of $P_0 = 1 \text{ ms}$, accreting $0.8M_\odot$ in fall-back matter over a timescale $t_{\text{fb}} = 3 \text{ s}$ (top panel) and $t_{\text{fb}} = 300 \text{ s}$ (bottom panel). Dashed lines show the same model, but neglecting the effects of fall-back. Vertical lines indicate the duration of the GRB prompt emission, defined as the interval $t_\sigma \sim T_{\text{GRB}}$ over which $100 \leq \sigma \leq 3000$. The effect of fall-back accretion is to lengthen the GRB duration from $\lesssim 100 \text{ s}$ for an isolated magnetar to $\sim 300 - 5000 \text{ s}$ in the accretion case.

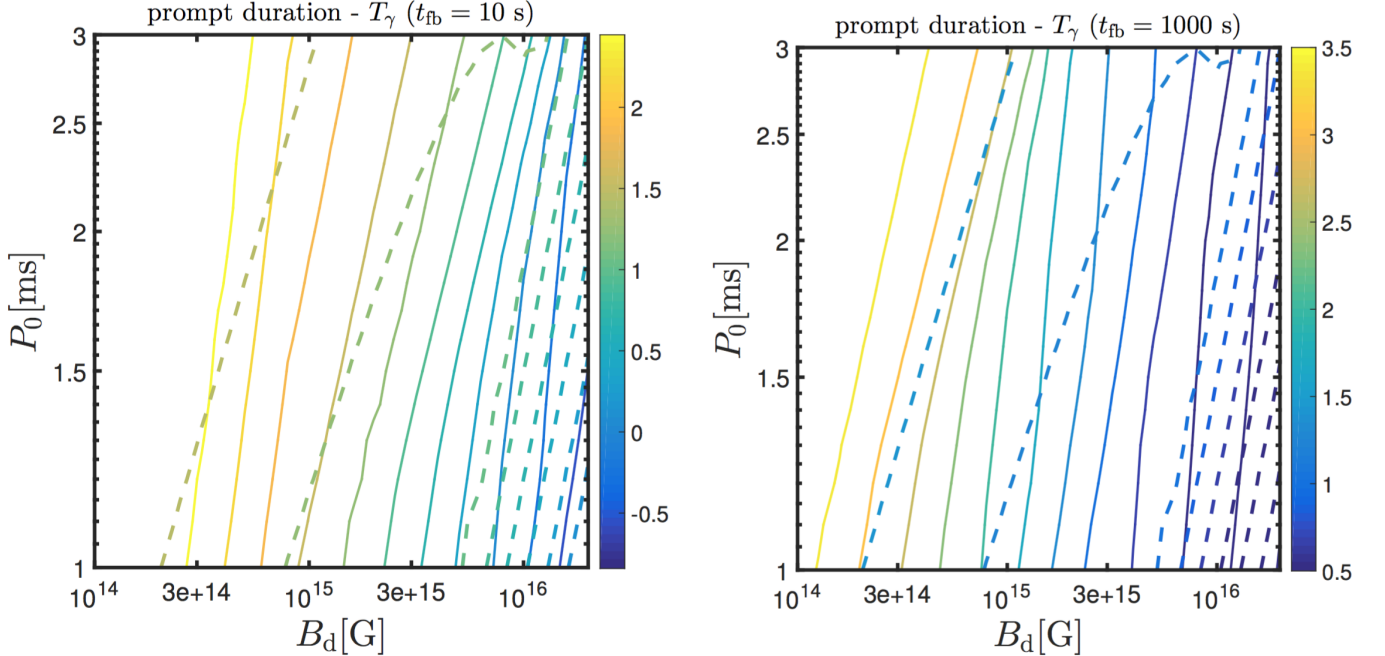


FIG. 8.— Accretion can substantially lengthen the duration of the prompt GRB emission across a wide range of the magnetar parameter space $B_d - P_0$. This figure shows the total duration of the GRB prompt emission, T_{GRB} , which we take to be the maximum between t_σ (the time interval over which the jet magnetization is in the range $\sigma = 100 - 3000$ necessary to produce prompt emission) and the magnetar spin-down time t_{sd} . We assume an initial NS mass of $1.4M_\odot$, an accreted mass of $0.8M_\odot$ and mass fall-back times $t_{\text{fb}} = 10 \text{ s}$ (top panel) or $t_{\text{fb}} = 1000 \text{ s}$ (bottom panel). Dashed lines depict the equivalent contours for a case with zero accretion. Note the change in the color bar range between the top and bottom figures.

completely, a binary NS merger is more likely to produce a quasi-stable supramassive NS remnant, which collapses to a black hole once its spin period increases above a critical period P_{collapse} , the precise value of which depends on

the mass of the remnant relative to the theoretically uncertain maximum mass of a non-rotating NS. [Margalit & Metzger \(2017\)](#) used energetic constraints on GW170817 to disfavor the formation of a long-lived supermassive NS

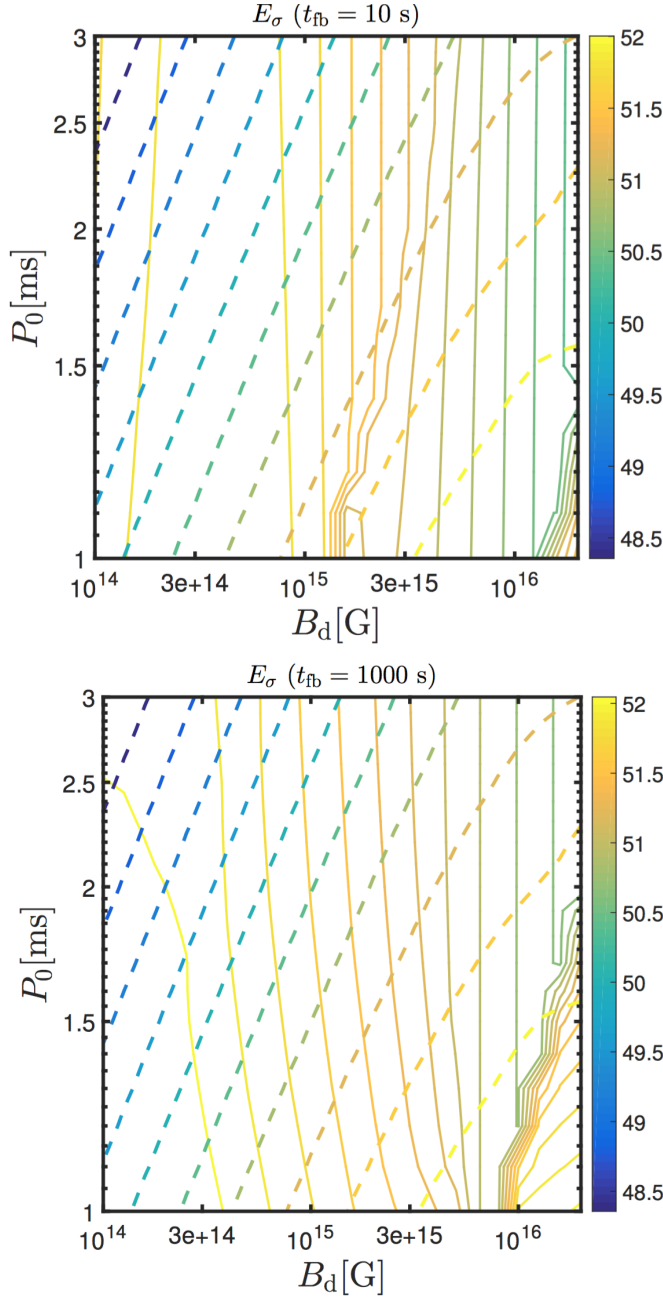


FIG. 9.— Accretion can enhance the total energy released during the prompt GRB emission across a wide range of the magnetar parameter space $B_d - P_0$. This figure shows the total rotational energy released by the magnetar wind in the magnetization range $\sigma = 100 - 3000$ necessary to produce prompt emission (e.g. Beniamini & Giannios 2017). We assume an initial NS mass of $1.4M_\odot$, an accreted mass of $0.8M_\odot$ and $t_{fb} = 10$ s (top panel) or $t_{fb} = 1000$ s (bottom panel). Dashed lines depict the equivalent contours for a case with no accretion.

remnant in this event by comparing the rotational energy released by an (isolated) NS as it spins down from an initial state close to the mass-shedding limit to the point of collapse, to observations constraining the kinetic energy of the GRB jet and kilonova ejecta. However, these constraints would be weakened if the surrounding accretion disk would substantially reduce the rotational energy released by the magnetar prior to its collapse.

Figure 11 shows the evolution of the cumulative extracted rotational energy for an accreting magnetar,

which demonstrates that, due to the transfer of angular momentum from the star to the disk, the energy in the magnetized wind released prior to the point of collapse ($P = P_{\text{collapse}}$) can be reduced by a factor of several relative to the otherwise identical case of an isolated magnetar. However, while including the accretion effects could weaken the constraints of Margalit & Metzger (2017) slightly, it would not significantly alter their quantitative conclusions regarding the maximum mass of the NS.

3.6. SLSNe

Powering a SLSN through the birth of an isolated magnetar requires one with a lower magnetic field strength, $B_d \lesssim \text{few} \times 10^{14}$ G, for which the spin-down timescale is comparable to the photon diffusion timescale outwards through the expanding supernova ejecta (Kasen & Bildsten 2010; Woosley 2010; Metzger et al. 2014). The contribution of the magnetar to the peak luminosity of the supernova is approximately given by the spin-down power evaluated at the time when the ejecta first becomes transparent to visual radiation, i.e. the characteristic diffusion timescale (Arnett 1982)

$$t_{\text{peak}} = \left(\frac{3\kappa M_{\text{ej}}}{4\pi c v_{\text{ej}}} \right)^{1/2} \approx 46 \text{ d} \left(\frac{M_{\text{ej}}}{10M_\odot} \right)^{1/2} \left(\frac{v_{\text{ej}}}{10^4 \text{ km s}^{-1}} \right)^{-1/2}, \quad (33)$$

where here $\kappa \approx 0.1 \text{ cm}^2 \text{ g}^{-1}$, M_{ej} and v_{ej} are the opacity, total mass and mean velocity of the ejecta, respectively; the latter can be approximated from the ejecta kinetic energy

$$\frac{M_{\text{ej}} v_{\text{ej}}^2}{2} = E_{\text{SN}} + \int_0^{t_{\text{peak}}} \dot{E}_{\text{sd}}, \quad (34)$$

which in general is a combination of the initial explosion energy $E_{\text{SN}} = 10^{51}$ ergs plus additional energy dumped into the ejecta by the magnetar prior to its transparency (Metzger et al. 2015; Soker & Gilkis 2017). Thus, the peak luminosity can be estimated as

$$L_{\text{peak}} \simeq \dot{E}_{\text{sd}}(t_{\text{peak}}) + L_{\text{Ni}}(t_{\text{peak}}), \quad (35)$$

where

$$L_{\text{Ni}} \approx 1.3 \times 10^{43} \text{ ergs s}^{-1} (M_{\text{Ni}}/0.2M_\odot) \exp(-t_{\text{peak}}/8.8\text{d}) \quad (36)$$

is the minimal contribution to the luminosity arising from the radioactive decay of ^{56}Ni of assumed mass M_{Ni} .

Figure 12 shows the peak luminosity of magnetar-powered SLSNe as a function of B_d and t_{fb} for $P_0 = 2$ ms, $M_{fb} = 0.8M_\odot$, $M_{\text{ej}} = 10M_\odot$. The peak luminosity is dominated by $\dot{E}_{\text{sd}}(t_{\text{peak}})$ and is typically in the range $L_{\text{peak}} \sim 10^{42} - 10^{45} \text{ ergs s}^{-1}$. Dashed lines show for comparison the luminosity in an otherwise equivalent case where accretion is negligible. For magnetars with $t_{fb} \ll t_{\text{peak}} \sim 3 \times 10^6$ s, the effects of accretion are to remove angular momentum from the magnetar and reduce the supernova luminosity, potentially below the SLSNe threshold $L_{\text{peak}} \sim 10^{44} \text{ ergs s}^{-1}$. On the other hand, for $t_{fb} \gtrsim t_{\text{peak}}$, the region of $B_d - P_0$ parameter space capable of producing SLSNe can be expanded. However, the stellar progenitors capable of producing such long fall-back times $t_{fb} \gtrsim 10^6 - 10^7$ s are blue supergiants with extended hydrogen-rich outer envelopes (Quataert & Kasen 2012),

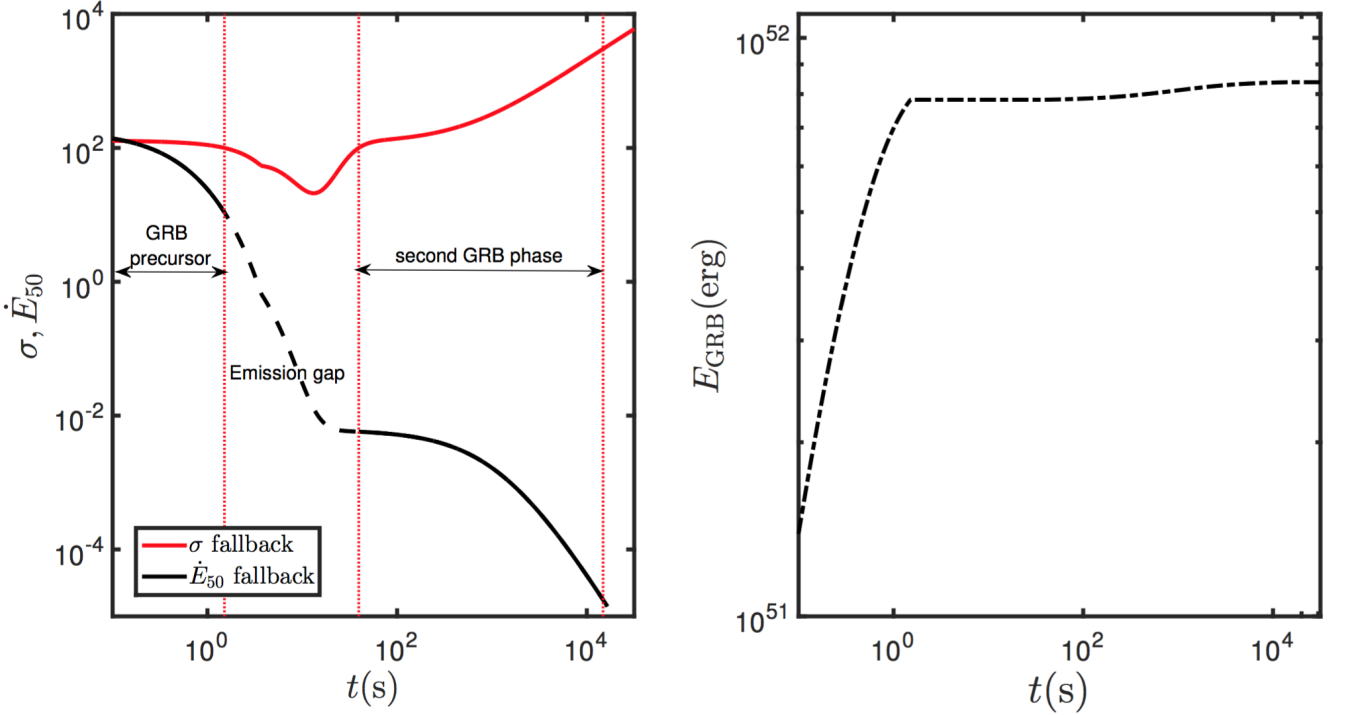


FIG. 10.— Magnetar jets can produce precursor episodes, followed by large gaps before the “main” emission episode. This figure shows the evolution of the spin-down power \dot{E} and magnetization σ of a magnetar wind for $B_d = 10^{16}$ G, $P_0 = 1$ ms which accretes $0.8M_\odot$ over a time $t_{\text{fb}} = 1000$. Energy released with a magnetization of $100 \leq \sigma \leq 3000$ is assumed to contribute to the GRB. Note that the non-monotonic evolution of σ results in the creation of a long temporal gap between the precursor and main emission episode. The right panel shows the cumulative energy deposited in the GRB phase E_{GRB} .

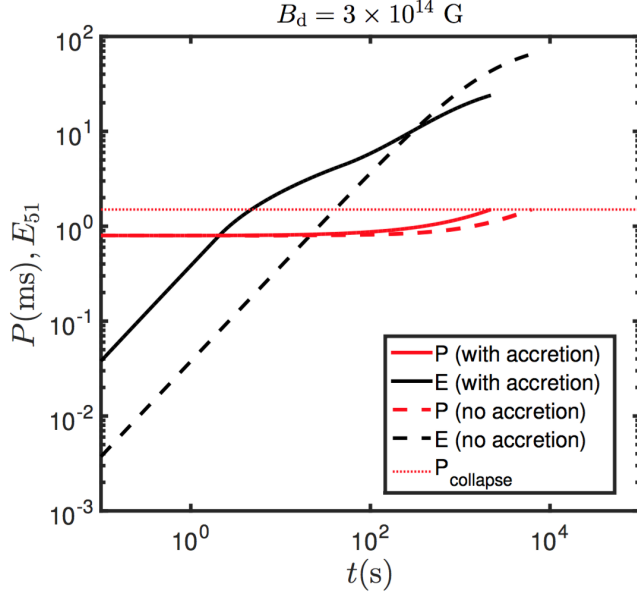


FIG. 11.— Time evolution of the cumulative extracted wind energy (black curves) and spin period (red curves) of a supramassive NS formed from a NS-NS merger. We assume an initial NS mass and spin of $M_{\text{NS}} = 2.4M_\odot$, $P = 0.8$ ms respectively as well as $M_{\text{fb}} = 0.1M_\odot$, $t_{\text{fb}} = 0.1$ s. The SMNS is assumed to collapse to a black hole once its period becomes slower than $P_{\text{collapse}} = 1.5$ ms (horizontal dashed line).

in tension with the hydrogen-poor classification of many SLSNe. Kinetic energy released in outflows from the accretion disk may provide a more promising source than the magnetar itself for powering SLSNe in the case of long

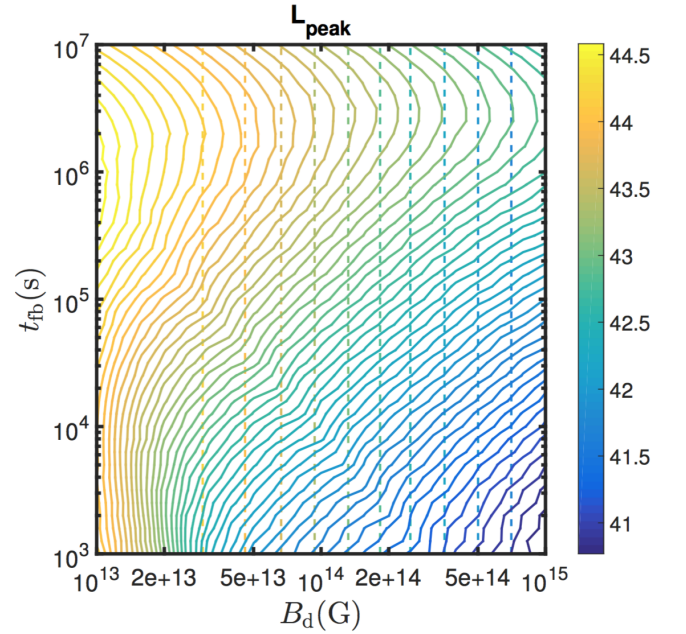


FIG. 12.— Peak luminosity of a magnetar-powered SLSNe (eq. 35) including the effects of accretion, as a function of surface dipole field B_d and fall-back time of the debris t_{fb} . All models assume an initial spin-period of $P_0 = 2$ ms, total accreted mass $M_{\text{acc}} = 0.8M_\odot$, and supernova ejecta mass $M_{\text{ej}} = 10M_\odot$. Colored dashed lines depict the peak luminosity for the otherwise identical case with no accretion.

fall-back times (e.g. Piro & Ott 2011; Dexter & Kasen 2013).

4. SUMMARY AND CONCLUSIONS

We have explored the effects of mass fall-back on the evolution of millisecond proto-magnetars formed in core collapse supernovae and neutron star mergers, comparing the evolution of their magnetized outflows and outflowed relativistic jets to the normally-considered case of an isolated (non-accreting) magnetar. Broadly, we find that adding accretion to the picture substantially expands the possible behavior of magnetar engines, alleviating some (but not all) of the observational or theoretical drawbacks present in the isolated magnetar model.

Our primary conclusions are summarized as follows:

- Fall-back accretion can appreciably alter the spin-down evolution of magnetars, even when the accreted mass is insufficient to instigate the gravitational collapse of the magnetar to a black hole.

Beyond enhancing (or reducing, in the propeller regime) the angular momentum of the star, the additional magnetic flux opened as the magnetosphere is compressed by accretion can greatly enhance the magnetar's spin-down luminosity (Fig. 1). One way to think about this is that accretion acts to increase the *effective* magnetic field strength entering the dipole spin-down formula by a factor (eqs. 12, 13)

$$\frac{B_{\text{eff}}}{B_d} = \frac{R_{\text{lc}}}{R_m} = \left(\frac{\dot{M}}{\dot{M}_{\text{lc}}} \right)^{2/7} \approx 2.15 P_{\text{ms}} B_{15}^{-4/7} \dot{M}_{-2}^{2/7} M_{1.4}^{-1/7}, \dot{M} \geq \dot{M}_{\text{lc}}. \quad (37)$$

The larger effective value of B_d when accretion is present has the implication that the magnetic field strength inferred by modeling the luminosity and timescale of the prompt emission phase (when \dot{M} is high) may not match the values inferred for the same events at later times, e.g. from the X-ray plateau phase (Rowlinson et al. 2013), once accretion has subsided (Fig. 13).

- Accretion generally drives the spin period towards a value $P_{\text{eq}}(t)$ corresponding to the condition $R_m = R_c$ (eq. 20). However, the details of whether this quasi-equilibrium is achieved depends on the precise coupling between the accretion disk and the NS magnetosphere, which remains an area of active debate even in the comparatively well-studied case of accreting pulsars.

When P_{eq} is obtained, the spin-down luminosity approaches a late-time decay $\dot{E}_{\text{sd}} \propto t^{-\alpha}$, where $\alpha = 1.90 - 2.38$ (eq. 25), moderately shallower or steeper than the standard $\dot{E}_{\text{sd}} \propto t^{-2}$ prediction for an isolated magnetar. Such differences might be observable on the post-maximum light curve decay of SLSNe (Nicholl et al. 2016), though this effect is degenerate with a decreasing fraction of the magnetar's energy being thermalized behind the ejecta (due to the growing fraction of UV, X-ray or gamma-ray radiation which directly escapes from the nebula without being reprocessed into optical emission; Metzger et al. 2014). The power-law decay might also be imprinted on the late-time X-ray

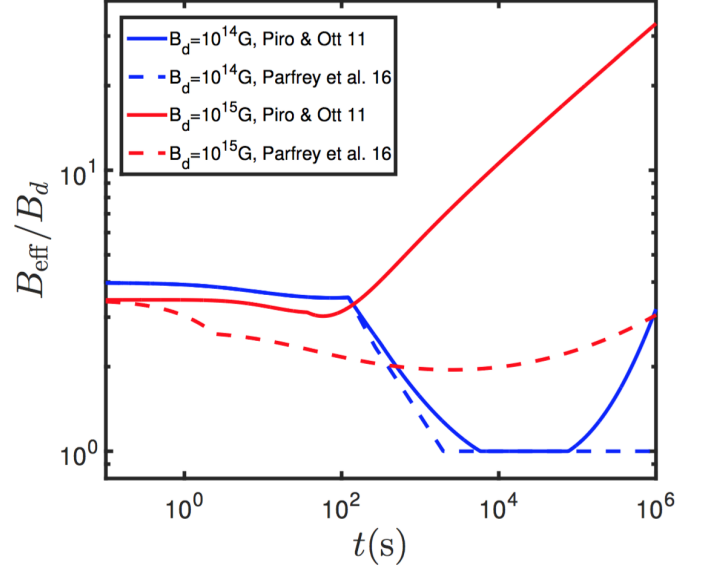


FIG. 13.— Time evolution of the effective dipole magnetic field strength (eq. 37) for purposes of calculating the magnetar spin-down luminosity when the effects of accretion are included, as shown for different surface dipole field strengths and fall-back times (assuming a total accreted mass of $0.8M_{\odot}$). A high value of B_{eff} at early times can explain a powerful GRB jet, which for the Parfrey et al. (2016) torque prescription, later decreases and could contribute to a long-lived X-ray plateau.

emission from GRBs (e.g. Rowlinson et al. 2013; Lasky et al. 2017), though this association depends on the possibly dubious assumption that the spin-down power faithfully tracks the isotropic X-ray luminosity.

- Accretion does not substantially enhance the maximum extractable rotational energy from a magnetar (Fig. 5) as compared to the case of an isolated (non-accreting) magnetar which is born maximally spinning, near break-up, $P_0 \simeq 1$ ms. This is because the amount of accreted mass required to maintain $P = P_{\text{eq}} \lesssim 1$ ms for many spin-down times exceeds that which would instigate collapse to a black hole (see eq. 27 and surrounding discussion). The concordance between the supernova energy scale of $\approx \text{few} \times 10^{52}$ ergs used by some authors to favor a magnetar origin for long GRB (Mazzali et al. 2014) remains preserved, if not strengthened, when accretion is included.

The propeller wind itself could carry away a substantial amount of kinetic energy (e.g. Piro & Ott 2011; Gompertz et al. 2014). However, such an outflow would be slower and more heavily baryon-loaded than the magnetar wind and thus cannot contribute to the ultra-relativistic GRB jet (though it could contribute to powering SLSNe for long fall-back times). Tension thus remains between the magnetar model and the most energetic GRBs (Cenko et al. 2011; Beniamini et al. 2017).

Perhaps more importantly, by contributing angular momentum to an initially slowly-spinning star, and by enhancing the spin-down luminosity compared to the isolated dipole (eq. 14, 37), accretion does substantially increase the parameter space of mag-

- netar birth properties (B_d, P_0) which could give rise to the production of a long GRB jet (Fig. 9). Accretion thus reduces the gap between the properties of magnetars which were previously thought capable of giving rise to GRBs versus SLSNe (Metzger et al. 2015; Margalit et al. 2018). The difference between GRB- and SLSN-producing magnetars could have as much or more to do with the fall-back accretion history they experience than with intrinsic differences in the magnetar birth properties.
- The gravitational energy liberated by accretion results in a persistent source of neutrino irradiation of the magnetar polar cap, supplying an additional source of neutrino-driven mass-loss than would be present from an isolated cooling magnetar (Fig. 2). Accretion thus maintains the baryon loading of the magnetar jet in the requisite range (magnetization $\sigma \lesssim 10^3$) to produce prompt emission for timescales $\sim 10^2 - 10^4$ s, much longer than the Kelvin-Helmholtz cooling timescale of the star, thereby increasing the maximum duration of GRB prompt emission to the range of ultra-long GRBs (Fig. 7, 8). This supports the possibility that GRB 111209A/SN2011kl (Greiner et al. 2015) represents the transitional case of a magnetar with an intermediate spin-down timescale $t_{\text{sd}} \sim 10^4$ s, which powered both the prompt GRB phase and later the SLSNe emission by re-energizing the supernova ejecta (Metzger et al. 2015; Gompertz & Fruchter 2017). By slowing the rate at which the jet magnetization $\sigma(t)$ rises at late times, this also alleviates tension between the rapid spectral evolution of prompt GRB emission predicted by isolated magnetar models and observations (Metzger et al. 2011; Beniamini et al. 2017).
 - Accretion allows for more complex time evolution of the magnetar spin-down power and wind baryon-loading (magnetization), which can in turn enable more complicated GRB light curve behavior than the smooth monotonic evolution predicted for an isolated magnetar. This additional freedom might help explain long GRBs with bright precursors which are followed by large temporal gaps before the main prompt emission episode (Fig. 10). The enhanced spin-down rate of an accreting magnetar could also enable a large jet power in the first $\lesssim 1$ s after the supernova explosion (as needed to

produce sufficient radioactive ^{56}Ni through shock-heating of the progenitor envelope) while spinning down at a more gradual rate over the subsequent tens of seconds or longer as the accretion rate subsides, as needed for producing the longer duration of the GRB (Fig. 6).

- An accreting millisecond magnetar could also be present in the aftermath of a binary NS merger. The accretion rate can be sufficiently high at early times to push the Alfvén radius down to the neutron star surface and open the magnetosphere into a monopole-like field structure (Metzger et al. 2018). However, because the disk is short-lived, its overall impact on the angular momentum and rotational energy budget of the magnetar is relatively minor. Still, angular momentum extracted by the disk would reduce the energy released into the surrounding environment from the magnetar wind (Fig. 11). This could moderately weaken energetic constraints which can be placed on the equation of state of the NS based on the type of compact remnant created in gravitational wave-detected mergers (Margalit & Metzger 2017). It would also impact inferences about the existence of stable magnetar remnants following short gamma-ray bursts based on their late-time radio emission (Metzger & Bower 2014; Horesh et al. 2016; Fong et al. 2016).
- The effect of mass accretion in magnetar-powered SLSNe is generally to reduce the rotational energy available to power the supernova if the fall-back time is shorter than the peak timescale of the SN of typically \approx weeks. Longer fall-back times could enhance the SLSNe emission; however, the more radially extended progenitor stars required to give such late fall-back should possess hydrogen envelopes, in tension with the Type I classification of engine-powered SLSNe (however, see Sukhbold & Thompson 2017).

BDM acknowledges support from NASA grants NNX16AB30G and NNX17AK43G issued through the Astrophysics Theory Program. DG acknowledges support from NASA grants NNX16AB32G and NNX17AG21G issued through the Astrophysics Theory Program

REFERENCES

- Abbott, B. P., Abbott, R., Abbott, T. D., et al. 2017a, *ApJ*, **848**, L13
- . 2017b, *Physical Review Letters*, **119**, 161101
- Aloy, M.-Á., Cuesta-Martínez, C. F., & Obergaulinger, M. 2018, ArXiv e-prints, [arXiv:1801.06186](https://arxiv.org/abs/1801.06186) [astro-ph.HE]
- Arnett, W. D. 1982, *ApJ*, **253**, 785
- Barnes, J., Duffell, P. C., Liu, Y., et al. 2017, ArXiv e-prints, [arXiv:1708.02630](https://arxiv.org/abs/1708.02630) [astro-ph.HE]
- Beniamini, P., & Giannios, D. 2017, *MNRAS*, **468**, 3202
- Beniamini, P., Giannios, D., & Metzger, B. D. 2017, *MNRAS*, **472**, 3058
- Beniamini, P., & Mochkovitch, R. 2017, *A&A*, **605**, A60
- Beniamini, P., Nava, L., Duran, R. B., & Piran, T. 2015, *MNRAS*, **454**, 1073
- Bernardini, M. G., Campana, S., Ghisellini, G., et al. 2013, *ApJ*, **775**, 67
- Bernardini, M. G., et al. 2014, *MNRAS*, **439**, L80
- Boër, M., Gendre, B., & Stratta, G. 2015, *ApJ*, **800**, 16
- Bromberg, O., Nakar, E., Piran, T., & Sari, R. 2011, *ApJ*, **740**, 100
- Bromberg, O., & Tchekhovskoy, A. 2016, *MNRAS*, **456**, 1739
- Bromberg, O., Tchekhovskoy, A., Gottlieb, O., Nakar, E., & Piran, T. 2017, ArXiv e-prints, [arXiv:1710.05897](https://arxiv.org/abs/1710.05897) [astro-ph.HE]
- Bucciantini, N., Metzger, B. D., Thompson, T. A., & Quataert, E. 2012, *MNRAS*, **419**, 1537
- Bucciantini, N., Quataert, E., Arons, J., Metzger, B. D., & Thompson, T. A. 2007, *MNRAS*, **380**, 1541

- Bucciantini, N., Quataert, E., Metzger, B. D., et al. 2009, *MNRAS*, **396**, 2038
- Bucciantini, N., Thompson, T. A., Arons, J., Quataert, E., & Del Zanna, L. 2006, *MNRAS*, **368**, 1717
- Burrows, A., & Lattimer, J. M. 1986, *ApJ*, **307**, 178
- Burrows, D. N., Grupe, D., Capalbi, M., et al. 2006, *ApJ*, **653**, 468
- Cenko, S. B., et al. 2011, *ApJ*, **732**, 29
- Chatzopoulos, E., Wheeler, J. C., Vinko, J., Horvath, Z. L., & Nagy, A. 2013, *ApJ*, **773**, 76
- Chevalier, R. A. 1989, *ApJ*, **346**, 847
- Contopoulos, I., Kazanas, D., & Fendt, C. 1999, *ApJ*, **511**, 351
- Dai, Z. G., & Lu, T. 1998, *A&A*, **333**, L87
- D’Angelo, C. R., & Spruit, H. C. 2012, *MNRAS*, **420**, 416
- Dessart, L., Hillier, D. J., Li, C., & Woosley, S. 2012, *MNRAS*, **424**, 2139
- Dexter, J., & Kasen, D. 2013, *ApJ*, **772**, 30
- Dong, S., et al. 2016, *Science*, **351**, 257
- Duncan, R. C., & Thompson, C. 1992, *ApJ*, **392**, L9
- Fenimore, E. E., Epstein, R. I., & Ho, C. 1993, *A&AS*, **97**, 59
- Fernández, R., Foucart, F., Kasen, D., et al. 2017, *Classical and Quantum Gravity*, **34**, 154001
- Fernández, R., & Metzger, B. D. 2013, *MNRAS*, **435**, 502
- Fong, W., Metzger, B. D., Berger, E., & Özel, F. 2016, *ApJ*, **831**, 141
- Fryer, C. L., Brown, P. J., Bufano, F., et al. 2009, *ApJ*, **707**, 193
- Gao, H., Ding, X., Wu, X.-F., Dai, Z.-G., & Zhang, B. 2015, *ApJ*, **807**, 163
- Gendre, B., Stratta, G., Atteia, J. L., et al. 2013, *ApJ*, **766**, 30
- Ghirlanda, G., Nava, L., Ghisellini, G., et al. 2012, *MNRAS*, **420**, 483
- Ghosh, P., & Lamb, F. K. 1978, *ApJ*, **223**, L83
- Giacomazzo, B., & Perna, R. 2013, *ApJ*, **771**, L26
- Gibson, S. L., Wynn, G. A., Gompertz, B. P., & O’Brien, P. T. 2017, *MNRAS*, **470**, 4925
- Gompertz, B., & Fruchter, A. 2017, *ApJ*, **839**, 49
- Gompertz, B. P., O’Brien, P. T., & Wynn, G. A. 2014, *MNRAS*, **438**, 240
- Greiner, J., et al. 2014, *A&A*, **568**, A75
- . 2015, *Nature*, **523**, 189
- Gungor, C., Ekşi, K. Y., Gougucs, E., & Guver, T. 2017, *ApJ*, **848**, 13
- Heger, A., Woosley, S. E., & Spruit, H. C. 2005, *ApJ*, **626**, 350
- Horesh, A., Hotokezaka, K., Piran, T., Nakar, E., & Hancock, P. 2016, *ApJ*, **819**, L22
- Hotokezaka, K., Kiuchi, K., Kyutoku, K., et al. 2013, *Phys. Rev. D*, **87**, 024001
- Kann, D. A., et al. 2016, ArXiv e-prints, [arXiv:1606.06791](https://arxiv.org/abs/1606.06791) [[astro-ph.HE](https://arxiv.org/archive/ph)]
- Kargatis, V. E., Liang, E. P., Hurley, K. C., et al. 1994, *ApJ*, **422**, 260
- Kasen, D., & Bildsten, L. 2010, *ApJ*, **717**, 245
- Kiuchi, K., Kyutoku, K., Sekiguchi, Y., Shibata, M., & Wada, T. 2014, *Phys. Rev. D*, **90**, 041502
- Kulkarni, S. R. 2005, ArXiv Astrophysics e-prints, [arXiv:astro-ph/0510256](https://arxiv.org/abs/astro-ph/0510256)
- Kumar, P., Narayan, R., & Johnson, J. L. 2008, *MNRAS*, **388**, 1729
- Lai, D., & Shapiro, S. L. 1995, *ApJ*, **442**, 259
- Lasky, P. D., Leris, C., Rowlinson, A., & Glampedakis, K. 2017, *ApJ*, **843**, L1
- Lattimer, J. M., & Schutz, B. F. 2005, *ApJ*, **629**, 979
- Lazzati, D. 2005, *MNRAS*, **357**, 722
- Leloudas, G., et al. 2016, *Nature Astronomy*, **1**, 0002
- Levan, A. J. 2015, ArXiv e-prints, [arXiv:1506.03960](https://arxiv.org/abs/1506.03960) [[astro-ph.HE](https://arxiv.org/archive/ph)]
- Levan, A. J., et al. 2014, *ApJ*, **781**, 13
- Liang, E.-W., Yi, S.-X., Zhang, J., et al. 2010, *ApJ*, **725**, 2209
- Lithwick, Y., & Sari, R. 2001, *ApJ*, **555**, 540
- Liu, Y.-Q., Modjaz, M., & Bianco, F. B. 2016, ArXiv e-prints, [arXiv:1612.07321](https://arxiv.org/abs/1612.07321) [[astro-ph.HE](https://arxiv.org/archive/ph)]
- Lü, H.-J., & Zhang, B. 2014, *ApJ*, **785**, 74
- Lü, J., Zou, Y.-C., Lei, W.-H., et al. 2012, *ApJ*, **751**, 49
- Margalit, B., & Metzger, B. D. 2017, *ApJ*, **850**, L19
- Margalit, B., Metzger, B. D., Thompson, T. A., Nicholl, M., & Sukhbold, T. 2018, *MNRAS*, [arXiv:1705.01103](https://arxiv.org/abs/1705.01103) [[astro-ph.HE](https://arxiv.org/archive/ph)]
- Margutti, R., Metzger, B. D., Chornock, R., et al. 2017, *ApJ*, **836**, 25
- Margutti, R., et al. 2018, ArXiv e-prints, [arXiv:1801.03531](https://arxiv.org/abs/1801.03531) [[astro-ph.HE](https://arxiv.org/archive/ph)]
- Mazzali, P. A., McFadyen, A. I., Woosley, S. E., Pian, E., & Tanaka, M. 2014, *MNRAS*, **443**, 67
- Metzger, B. D., Arcones, A., Quataert, E., & Martínez-Pinedo, G. 2010, *MNRAS*, **402**, 2771
- Metzger, B. D., & Bower, G. C. 2014, *MNRAS*, **437**, 1821
- Metzger, B. D., & Fernández, R. 2014, *MNRAS*, **441**, 3444
- Metzger, B. D., Giannios, D., Thompson, T. A., Bucciantini, N., & Quataert, E. 2011, *MNRAS*, **413**, 2031
- Metzger, B. D., Margalit, B., Kasen, D., & Quataert, E. 2015, *MNRAS*, **454**, 3311
- Metzger, B. D., & Piro, A. L. 2014, *MNRAS*, **439**, 3916
- Metzger, B. D., Piro, A. L., & Quataert, E. 2008a, *MNRAS*, **390**, 781
- . 2009, *MNRAS*, **396**, 1659
- Metzger, B. D., Quataert, E., & Thompson, T. A. 2008b, *MNRAS*, **385**, 1455
- Metzger, B. D., Thompson, T. A., & Quataert, E. 2007, *ApJ*, **659**, 561
- . 2018, ArXiv e-prints, [arXiv:1801.04286](https://arxiv.org/abs/1801.04286) [[astro-ph.HE](https://arxiv.org/archive/ph)]
- Metzger, B. D., Vurm, I., Hascoët, R., & Beloborodov, A. M. 2014, *MNRAS*, **437**, 703
- Milosavljević, M., Lindner, C. C., Shen, R., & Kumar, P. 2012, *ApJ*, **744**, 103
- Moriya, T. J., Metzger, B. D., & Blinnikov, S. I. 2016, *ApJ*, **833**, 64
- Morsony, B. J., Lazzati, D., & Begelman, M. C. 2010, *ApJ*, **723**, 267
- Mösta, P., Richers, S., Ott, C. D., et al. 2014, *ApJ*, **785**, L29
- Nicholl, M., Guillochon, J., & Berger, E. 2017, ArXiv e-prints, [arXiv:1706.00825](https://arxiv.org/abs/1706.00825) [[astro-ph.HE](https://arxiv.org/archive/ph)]
- Nicholl, M., et al. 2016, *ApJ*, **828**, L18
- Parfrey, K., Spitkovsky, A., & Beloborodov, A. M. 2016, *ApJ*, **822**, 33
- Perna, R., Duffell, P., Cantiello, M., & MacFadyen, A. I. 2014, *ApJ*, **781**, 119
- Piro, A. L., & Ott, C. D. 2011, *ApJ*, **736**, 108
- Pons, J. A., Reddy, S., Prakash, M., Lattimer, J. M., & Miralles, J. A. 1999, *ApJ*, **513**, 780
- Pooley, D., Kumar, P., & Wheeler, J. C. 2017, ArXiv e-prints, [arXiv:1712.03240](https://arxiv.org/abs/1712.03240) [[astro-ph.HE](https://arxiv.org/archive/ph)]
- Price, D. J., & Rosswog, S. 2006, *Science*, **312**, 719
- Qian, Y., & Woosley, S. E. 1996, *ApJ*, **471**, 331
- Quataert, E., & Kasen, D. 2012, *MNRAS*, **419**, L1
- Romanova, M. M., Ustyugova, G. V., Koldoba, A. V., & Lovelace, R. V. E. 2004, *ApJ*, **616**, L151
- Romanova, M. M., Ustyugova, G. V., Koldoba, A. V., Wick, J. V., & Lovelace, R. V. E. 2003, *ApJ*, **595**, 1009
- Rosswog, S. 2007, *MNRAS*, **376**, L48
- Rowlinson, A., Gompertz, B. P., Dainotti, M., et al. 2014, *MNRAS*, **443**, 1779
- Rowlinson, A., O’Brien, P. T., Metzger, B. D., Tanvir, N. R., & Levan, A. J. 2013, *MNRAS*, **430**, 1061
- Rowlinson, A., et al. 2010, *MNRAS*, **409**, 1479
- Siegel, D. M., & Ciolfi, R. 2016a, *ApJ*, **819**, 14
- . 2016b, *ApJ*, **819**, 15
- Siegel, D. M., Ciolfi, R., Harte, A. I., & Rezzolla, L. 2013, *Phys. Rev. D*, **87**, 121302
- Soker, N., & Gilkis, A. 2017, *ApJ*, **851**, 95
- Spitkovsky, A. 2006, *ApJ*, **648**, L51
- Sukhbold, T., Ertl, T., Woosley, S. E., Brown, J. M., & Janka, H.-T. 2016, *ApJ*, **821**, 38
- Sukhbold, T., & Thompson, T. A. 2017, *MNRAS*, **472**, 224
- Suwa, Y., & Tominaga, N. 2015, *MNRAS*, **451**, 282
- Thompson, T. A. 2003, *ApJ*, **585**, L33
- Thompson, T. A., Chang, P., & Quataert, E. 2004, *ApJ*, **611**, 380
- Thompson, T. A., & ud-Doula, A. 2017, ArXiv e-prints, [arXiv:1709.03997](https://arxiv.org/abs/1709.03997) [[astro-ph.HE](https://arxiv.org/archive/ph)]
- Ugiano, M., Janka, H.-T., Marek, A., & Arcones, A. 2012, *ApJ*, **757**, 69
- Usov, V. V. 1992, *Nature*, **357**, 472
- Uzdensky, D. A., & MacFadyen, A. I. 2007, *ApJ*, **669**, 546
- Vlasov, A. D., Metzger, B. D., Lippuner, J., Roberts, L. F., & Thompson, T. A. 2017, *MNRAS*, **468**, 1522
- Vlasov, A. D., Metzger, B. D., & Thompson, T. A. 2014, *MNRAS*, **444**, 3537

- Wang, L.-J., Han, Y.-H., Xu, D., et al. 2016, [ApJ](#), **831**, 41
- Wang, X.-Y., & Mészáros, P. 2007, [ApJ](#), **670**, 1247
- Wheeler, J. C., Yi, I., Höflich, P., & Wang, L. 2000, [ApJ](#), **537**, 810
- Woods, E., & Loeb, A. 1995, [ApJ](#), **453**, 583
- Woosley, S. E. 2010, [ApJ](#), **719**, L204
- Woosley, S. E., & Bloom, J. S. 2006, [ARAA](#), **44**, 507
- Woosley, S. E., & Heger, A. 2012, [ApJ](#), **752**, 32
- Wu, X.-F., Hou, S.-J., & Lei, W.-H. 2013, [ApJ](#), **767**, L36
- Yu, Y.-W., Zhang, B., & Gao, H. 2013, ArXiv e-prints 1308.0876, [arXiv:1308.0876 \[astro-ph.SR\]](#)
- Yu, Y.-W., Zhu, J.-P., Li, S.-Z., Lü, H.-J., & Zou, Y.-C. 2017, [ApJ](#), **840**, 12
- Zhang, B. 2013, [ApJ](#), **763**, L22
- Zhang, B., & Mészáros, P. 2001, [ApJ](#), **552**, L35
- Zhang, D., & Dai, Z. G. 2010, [ApJ](#), **718**, 841
- Zhang, W., Woosley, S. E., & Heger, A. 2008, [ApJ](#), **679**, 639